Naval Research Laboratory
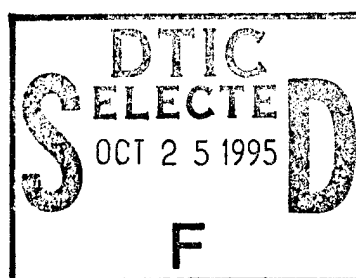Stennis Space Center, MS 39529-5004

Operation Rocky Road: Three-Dimensional Noise Field Directionality Estimation

RONALD A. WAGSTAFF
JOAL J. NEWCOMB

Ocean Acoustics Branch
Acoustics Division

DTIC
ELECTE
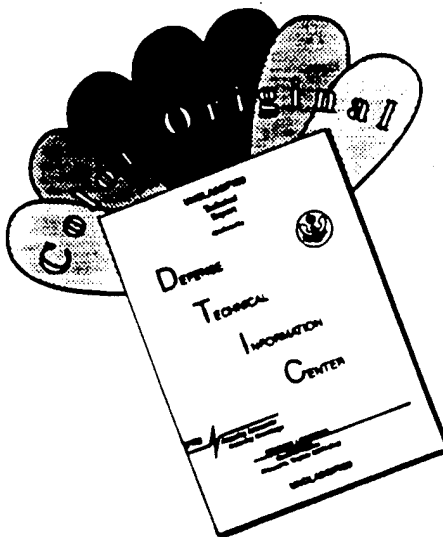OCT 2 5 1995
F

October 6, 1995

*Original contains color
plates: All DTIC reproduct-
ions will be in black and
white*

19951023 177

DTIC QUALITY INSPECTED 5

DISCLAIMER NOTICE

THIS DOCUMENT IS BEST QUALITY AVAILABLE. THE COPY FURNISHED TO DTIC CONTAINED A SIGNIFICANT NUMBER OF COLOR PAGES WHICH DO NOT REPRODUCE LEGIBLY ON BLACK AND WHITE MICROFICHE.

REPORT DOCUMENTATION PAGE		Form Approved OBM No. 0704-0188

Public reporting burden for this collection of information is estimated to average 1 hour per response, including the time for reviewing instructions, searching existing data sources, gathering and maintaining the data needed, and completing and reviewing the collection of information. Send comments regarding this burden or any other aspect of this collection of information, including suggestions for reducing this burden, to Washington Headquarters Services, Directorate for information Operations and Reports, 1215 Jefferson Davis Highway, Suite 1204, Arlington, VA 22202-4302, and to the Office of Management and Budget, Paperwork Reduction Project (0704-0188), Washington, DC 20503.

1. AGENCY USE ONLY *(Leave blank)*	2. REPORT DATE October 6, 1995	3. REPORT TYPE AND DATES COVERED Final

4. TITLE AND SUBTITLE

Operation Rocky Road: Three-Dimensional Noise Field Directionality Estimation

6. AUTHOR(S)

Ronald A. Wagstaff and Joal J. Newcomb

5. FUNDING NUMBERS

Job Order No. 571521406

Program Element No. 0602435N

Project No.

Task No. R035C91

Accession No.

7. PERFORMING ORGANIZATION NAME(S) AND ADDRESS(ES)

Naval Research Laboratory
Acoustics Division
Stennis Space Center, MS 39529-5004

8. PERFORMING ORGANIZATION REPORT NUMBER

NRL/MR/7176--95-7705

9. SPONSORING/MONITORING AGENCY NAME(S) AND ADDRESS(ES)

Office of Naval Research
800 N. Quincy St.
Arlington, VA 22217-5000

10. SPONSORING/MONITORING AGENCY REPORT NUMBER

11. SUPPLEMENTARY NOTES

12a. DISTRIBUTION/AVAILABILITY STATEMENT

Approved for public release; distribution unlimited.

12b. DISTRIBUTION CODE

13. ABSTRACT *(Maximum 200 words)*

For many reasons, the three-dimensional (3D) arrival structure of the undersea ambient noise field is of interest to the research and development community. One is that the arrival structure can be used to estimate the beam noise of an array, which may be required to estimate the performance of the array as an operational Navy asset or a scientific measurement tool. Another reason is that there are clues inherent in the vertical arrival structure that relate to the nature of the acoustic propagation along the azimuths of the noise sources. Similarly, there are also clues in the horizontal arrival structure of the undersea ambient noise field that relate to the azimuthal distribution of the noise sources. Both these classes of clues are important in the verification and validation of undersea ambient noise models. The ideal measurement tool to measure the 3D arrival structure of the noise field is a high resolution volumetric array sonar system. Unfortunately, such a system is not generally available. However, towed horizontal line arrays are available and can be used, even though they are far from ideal. The beam patterns of a line array are conically symmetric about the axis of the array. When the axis of a horizontal line array is tilted slightly from an elevation angle of 0 degree, the vertical character of the beam cones can be used to discriminate between various vertical arrival angles. Combined with measurements made on several different towed array headings, an estimate of the 3D directionality of the noise field can be obtained. An algorithm that uses such a technique on a single-line towed array data to generate an estimate of the 3D directionality of the noise field is described herein. Some results measured data from the ROCKY ROAD MILOC exercise are presented and discussed.

14. SUBJECT TERMS

ambient noise, shallow-water acoustics, full-spectrum processing, broadband, shipping noise, biological noise, wind noise

15. NUMBER OF PAGES
56

16. PRICE CODE

17. SECURITY CLASSIFICATION OF REPORT Unclassified	18. SECURITY CLASSIFICATION OF THIS PAGE Unclassified	19. SECURITY CLASSIFICATION OF ABSTRACT Unclassified	20. LIMITATION OF ABSTRACT SAR

CONTENTS

Accesion For		
NTIS CRA&I	☑	
DTIC TAB	☐	
Unannounced	☐	
Justification		
By		
Distribution /		
Availability Codes		
Dist	Avail and / or Special	
A-1		

OPERATION ROCKY ROAD: THREE-DIMENSIONAL NOISE FIELD DIRECTIONALITY ESTIMATION

by

R. A. Wagstaff and J. Newcomb
Naval Research Laboratory, SSC, MS 39529-5004, USA

ABSTRACT

For many reasons, the three dimensional (3D) arrival structure of the undersea ambient noise field is of interest to the research and development community. One is that the arrival structure can be used to estimate the beam noise of an array, which may be required to estimate the performance of the array as an operational Navy asset or a scientific measurement tool. Another reason is that there are clues inherent in the vertical arrival structure that relate to the nature of the acoustic propagation along the azimuths of the noise sources. Similarly, there are also clues in the horizontal arrival structure of the undersea ambient noise field that relate to the azimuthal distribution of the noise sources. Both of these classes of clues are important in the verification and validation of undersea ambient noise models. The ideal measurement tool to measure the 3D arrival structure of the noise field is a high resolution volumetric array sonar system. Unfortunately, such a system is not generally available. However, towed horizontal line arrays are available and can be used, even though they are far from ideal. The beam patterns of a line array are conically symmetric about the axis of the array. When the axis of a horizontal line array is tilted slightly from an elevation angle of 0 deg, the vertical character of the beam cones can be used to discriminate between various vertical arrival angles. Combined with measurements made on several different towed array headings, an estimate of the 3D directionality of the noise field can be obtained. An algorithm that uses such a technique on single-line towed array data to generate an estimate of the 3D directionality of the noise field is described herein. Some results using measured data from the ROCKY ROAD MILOC exercise are presented and discussed.

INTRODUCTION

In order to design sonar systems which operate with maximum effectiveness, it is necessary to understand as much as possible about the undersea ambient noise. Two characteristics of the noise that have been of particular concern in the past are its vertical and horizontal directionalities. Urick[1] gives an excellent summary of undersea ambient noise directionality measurements, and Etter[2] describes computer models that predict the

directional characteristics of the noise for various environmental and noise source input parameters. Unfortunately, these noise models are limited by the ability to accurately calculate the acoustic environment, to specify the radiation characteristics of the noise sources, and to predict their spatial distributions. The capabilities in some of these areas have improved considerably in the past few years, but have not advanced as much in other areas. For example, the development of the parabolic equation (PE) solution to the wave equation has greatly increased the ability to accurately calculate propagation in complex acoustic environments.[3] This, in turn, improves the ability to model the ambient noise in those environments. On the other hand, the complete radiation characteristics of ships are still not well understood. For example, the radiation directivity patterns of the noise caused by the cavitating screws are known to vary with elevation and azimuth angle and with screw depth, but a quantitative description for general classes of ships is not presently available. Hence, there are still enough uncertainties in various aspects of the prediction process, that the development of noise models will continue to be an ongoing process. As the noise models improve, the requirements on measured results to verify and validate the models will be more specific, and the nature of the processing of the noise measurement data to satisfy those specific needs will be much more demanding. A 3D noise field estimation technique used with current towed arrays might immediately satisfy some of the need for more complete information about the noise and partially alleviate some of the demand for measurements that require nonexistent multi-dimensional arrays.

In the past, conventional two dimensional (2D) results from vertical arrays, which integrate over azimuth, and from towed horizontal line arrays, which integrate over vertical arrival angle, have been adequate for noise model validation. This was because the greatest need has been to predict the performance of single line array sonar systems. However, multiple line array sonar systems, and even large multi-dimension array sonar systems, are now being considered and tested.[4-5] To predict the performance of these complex sonar systems, and other equally complex systems in the future, requires as much knowledge about the 3D arrival structure of the ambient noise as possible. This knowledge must be acquired from data measured with sonar systems in common use at the present time. The bulk of those measurements will, of necessity, be made with line arrays, including single-line towed arrays.

The horizontal single-line towed array is considered an excellent tool for measuring the 2D horizontal directionality of the ambient noise field. A common method of measurement is to tow the array on several different courses and use the beam noise measurements thus acquired to resolve the left-right ambiguities in the beam noise response patterns. These

2

data are usually processed by an algorithm that ignores the vertical dimension and confines itself entirely to the horizontal plane or azimuth dimension. Such an algorithm yields an estimate of the vertically integrated horizontal directionality of the ambient noise. Several techniques have been devised for resolving the left-right ambiguities and for producing 2D estimates of the noise field horizontal directionality. A few examples are presented and discussed in Refs. 6-11. All of the techniques, except the one in Ref. 11, ignore the vertical arrival structure of the noise. Furthermore, the technique in Ref. 11 only uses the vertical arrival structure to obtain a better estimate of the 2D horizontal structure of the noise field. None of the previous techniques known to the authors treat the horizontal and vertical dimensions as independent regimes.

The noise field 3D estimation technique discussed herein can be considered similar in concept to the two 2D techniques discussed in Refs. 10 and 11, but differs in implementation in two critical ways. First, it keeps the elevation (vertical) and azimuth (horizontal) dimensions independent. Second, it utilizes the entire 3D beam noise response patterns of the line array. This means that, with as little as one degree vertical tilt on the towed array, the measured vertical ambiguities can be resolved. A tilted towed array condition is easily met, since the towed array is seldom exactly horizontal during measurements. Thus, by maintaining the vertical and horizontal independence, the technique discussed herein can produce an estimate of the complete 3D directionality of the ambient noise field.

The next section provides a brief background discussion. The section that follows describes the 3D noise field directionality estimation technique. That section is followed by a discussion of some results, and then observations and conclusions are given.

BACKGROUND

Knowledge of the 3D structure of the undersea ambient noise is of value for a number of reasons. From a scientific perspective, the vertical arrival structure measured by a vertical array tells something about the average acoustic propagation conditions along a particular azimuth. Analogously, the azimuthal arrival structure, measured by a horizontal array, tells something about the azimuthal distribution of the noise sources. Even when the results of these two types of arrays are used together (incoherently), there will be blind spots in the noise sphere (or 3D space) that cannot be estimated with a 2D analysis. Such blind spots could, in fact, be measured by a 2D or 3D array. Hence, a technique that can estimate the 3D structure of the noise field from more readily available, and more easily

acquired, single-line towed array data would provide information now to enable the sonar design engineer to design future multidimensional (2D or 3D) arrays, as well as to predict their performance.

The vertical line array is well suited for measuring the vertical directionality of the ambient noise. However, its conical beam responses are formed about a vertical axis, and they integrate the arrivals from all azimuth angles received at a given elevation angle. Unfortunately, the beams cannot distinguish one arrival at a given azimuth from another at a different azimuth with the same elevation angle. The horizontal line array has a different limitation. Its conical beams are formed along a horizontal axis, and have both azimuth and elevation angle dependence. Some techniques have been devised to utilize the beam noise measured, with the horizontal array on different headings, to estimate the horizontal directionality of the ambient noise.[6-11] However, each of these techniques, except the technique in Ref. 11, assumes that the ambient noise is concentrated in the horizontal plane (i.e., no vertical arrival structure). The technique in Ref. 11 differs substantially from the others, in that it utilizes an estimate of the shape of the azimuthally averaged ambient noise vertical directionality, similar to that provided by a vertical line array, to improve the estimate of the horizontal directionality. However, it does not produce a 3D estimate of the ambient noise, just a better estimate of the 2D horizontal directionality. In the process, it reduces the error caused by ignoring the vertical arrival structure of the ambient noise. Hence, the technique in Ref. 11 is a substantial improvement over the other techniques, but it falls short of the desired 3D estimate of the noise field.

Acquiring a measurement of the 3D structure of the noise is not a simple task. Generally, a multidimensional array would be required, but these arrays are usually expensive to construct and difficult to deploy. On the other hand, the single-line towed array is extremely easy to deploy, sometimes requiring less than 1 hour for deployment and usually not much more than that to achieve a stable towing condition. However, it has the limitation of conical beams, rather than the "ideal searchlight" beams of a volumetric array. The technique presented in this paper overcomes, to some degree, the conical limitation of the single-line towed array beams, and provides an estimate of the 3D structure of the ambient noise field. Such an estimate can be used in the design and performance prediction of simple and complex sonar systems, including systems that have multidimensional arrays.

4

APPROACH

It is assumed that the ambient noise $N(\theta,\phi,t)$ can be expressed as:

$$N(\theta,\phi,t) = n(\theta,\phi) + \zeta(\theta,\phi,t) + \varepsilon(\theta,\phi,t) \ , \qquad (1)$$

where

θ is the spherical angle in azimuth,

ϕ is the spherical angle in elevation,

t is time,

$n(\theta,\phi)$ is the pseudo-stationary 3D background noise field directionality,

$\zeta(\theta,\phi,t)$ is the time dependent component of the noise due to fluctuations in acoustic propagation, noise source movement, changes in noise source levels, etc., and

$\varepsilon(\theta,\phi,t)$ is the error introduced in the measurements by the towship noise, array nonlinearities, flow noise, system faults, etc.

The technique presented herein attempts to estimate the pseudo-stationary 3D background directionality term $n(\theta,\phi)$ in Eq. 1. This term is considered herein to be more characteristic of what most present noise models attempt to predict. With sufficient temporal averaging, the influence of the fluctuating component $\zeta(\theta,\phi,t)$ can be considered negligible. However, if the performance of a signal processor is to be predicted (not the case here), the importance of $\zeta(\theta,\phi,t)$ cannot be overemphasized. Furthermore, it is assumed that the error component $\varepsilon(\theta,\phi,t)$ can be made acceptably small by array grooming and appropriate error discrimination processing techniques.

The data from which $n(\theta,\phi)$ is estimated (see Ref. 11) is the set of beam-output noise intensities measured by the ith beam while on the jth array heading. This can be represented as

$$r_{i,j} = \frac{1}{T}\int_0^T \frac{1}{2\pi}dt \int_0^{2\pi} \frac{1}{2}d\theta \int_{-\pi/2}^{\pi/2} N(\theta,\phi,t)b_i(\theta - \gamma_j,\phi)\cos\phi \, d\phi \ , \qquad (2)$$

where

T is the measurement time interval,

$b_i(\theta,\phi)$ is the ith beam response pattern of I beams, and

γ_j is the jth array heading of J array headings.

With temporal averaging, array grooming, and error discrimination processing techniques, Eq. 2 reduces to

$$r_{i,j} \approx \frac{1}{4\pi} \int\limits_0^{2\pi} d\theta \int\limits_{-\pi/2}^{\pi/2} n(\theta,\phi) b_i(\theta - \gamma_j, \phi) \cos\phi \, d\phi . \tag{3}$$

Here, $n(\theta,\phi)$ is obtained indirectly by forming an initial guess $\hat{n}_0(\theta,\phi)$ (which could simply be a constant value for all θ and ϕ, i.e., isotropic noise), substituting $\hat{n}_0(\theta,\phi)$ in place of $n(\theta,\phi)$ in Eq. 3, and then performing the integration to get an initial estimate $\hat{r}_{i,j,0}$ for each beam and array heading. The differences

$$\Delta_{i,j,0} = r_{i,j} - \hat{r}_{i,j,0} \tag{4}$$

are accumulated for all θ and ϕ within the response footprint of the ith beam on the jth array heading for all I beams and J array headings. The $\Delta_{i,j,0}$ are used to modify $\hat{n}_0(\theta,\phi)$ to create a new estimate $\hat{n}_1(\theta,\phi)$, which is again used in Eq. 3. This is an iterative process that is continued until the $\Delta_{i,j,k}$ (where k is number of iterations) are less than some arbitrary small value.

The iterative technique just described is not limited to towed array data, although much emphasis is placed on its use. In fact, data from any array can be used in the 3D noise field estimation algorithm, so long as the corresponding 3D beam response pattern of the array is available. For example, an improved estimate of the 3D arrival structure of the noise field could be achieved by supplementing towed array data with data acquired concurrently from a vertical line array. This special case will be demonstrated by the results presented herein. The vertical array may have different beam patterns and a different number of beams than the towed array, but such differences are inherently covered by the generic nature of Eq. 3. As far as the 3D estimation algorithm is concerned, the vertical array data is simply another data set with different beam patterns. In the extreme, even the data from a 3D array could be used. In such a case, the 3D algorithm would still deconvolve the beam patterns from the data and produce an improved deconvolved estimate of the 3D noise field.

Figure 1 illustrates the 3D response of four different beams. The beam noise response spheres, as well as the 3D ambient noise field, are represented as planes (similar to a "flat earth" plot or a Mercator projection) with the elevation angles ϕ plotted along the vertical axis, and the azimuth angles θ plotted along the horizontal axis. Figure 1a shows the beam response near aft endfire for a horizontal line array towed on a heading of 50 deg.

The multi-colored region gives the beam response level of the main lobe. The complete beam response pattern, including the sidelobes, has not been presented to avoid excessive clutter in the plots. However, the complete patterns are used in the algorithm, and in generating the results discussed below. Figure 1b shows a similar response for the broadside beam of the same array. The beam response in Fig. 1b covers all azimuth angles at ±90 deg because it contains both the "north and south" poles. When the line array is tilted relative to the horizontal plane, as in Fig. 1c for a vertical tilt angle of 30 deg, the response pattern no longer contains the north and south poles. Instead, it forms a serpentine pattern about the equator (0 deg elevation angle), and covers a region in the vertical that is approximately equal to 180 deg minus twice the tilt angle. Figure 1d shows the beam response for a beam steered 56 deg from forward endfire, when the array has a vertical tilt angle of 30 deg. This plot is reminiscent of a broken pair of eye glasses. As a general rule, the beam patterns in the rectangular display of the θ - ϕ domain are rather complicated. However, they can be calculated once and stored for repeated use in the iterative process during the generation of the estimate $\hat{n}_k(\theta,\phi)$.

The set of beam response patterns is calculated in spherical space by transforming the intersection of the conical pattern with a unit sphere by the following transformation.[11]

$$\beta = \cos^{-1}\left\{\cos\theta\cos\phi\cos\alpha + \sin\left[\cos^{-1}(\cos\theta\cos\phi)\right]\sin\alpha\right.$$
$$\left.\sin\left[\tan^{-1}(\sin\phi\,/\cos\phi\sin\theta)\right]\right\},\tag{5}$$

where
$\quad\beta$ is the conical angle of a differential element on the surface of a unit sphere, and

$\quad\alpha$ is the tilt angle of the array.

Figure 2 illustrates the geometry of Eq. 5 (Ref. 11 gives a more complete discussion).

The generation of the 3D noise field directionality estimate can be summarized as follows:

- assume a 3D noise field (e.g., isotropic, $\hat{n}_0(\theta,\phi) = C$),
- transform the spherical noise field to the conical field of the array (e.g., use Eq. 5),
- obtain beam noise estimates $\hat{r}_{i,j,0}$ using $\hat{n}_0(\theta,\phi)$,
- compare resulting beam noise estimates $\hat{r}_{i,j,0}$ with measured beam noise $r_{i,j}$,

- modify $\hat{n}_0(\theta, \phi)$ at all cells in the θ - ϕ domain, within the coverage footprint of the beam, according to the differences $\Delta_{i,j,0} = r_{i,j} - \hat{r}_{i,j,0}$ to get a new estimate $\hat{n}_1(\theta, \phi)$, and
- Repeat the above procedure until acceptable agreement is achieved (the $\Delta_{i,j,k}$ are less than some arbitrary small value).

RESULTS

Ambient noise measurements were made by a horizontal single-line towed array at seven locations near and in the Vestfjørd, Norway, during August and September 1993. In addition, ambient noise measurements were made concurrently at three of these locations with a vertical line array. Both arrays were SACLANT Centre equipment, and were deployed from the SACLANT Centre's ship the R/V ALLIANCE. These measurements were done in support of, and in conjunction with, one phase of the NATO multi-nation Military Oceanographic (MILOC) exercise RESOLUTE SUPPORT,[12] designated ROCKY WATER 93/9[13]. The results discussed herein were obtained using data from one of the sites inside the Vestfjørd (site A or polygon 7), and two of the sites outside the Vestfjørd in relatively shallow water (site D or polygon 1, and site E or polygon 4). Figure 3 is an illustration of the bathymetry in the Vestfjørd area, with the general site of the measurements as labeled.

Towed horizontal line array beam noise data were collected at each site on at least nine different array headings (i.e., nine legs). The headings of the legs were appropriately spaced in azimuth to insure a reasonable sampling. The towed array generally had a tilt from the horizontal (0 deg elevation angle) of approximately 1 to 2 deg. The tilt of the towed array is used by the algorithm to help resolve the up-down ambiguities of the conical beams. In addition, a vertical line array was deployed, and data were measured, at each of the three sites concurrently with at least five of the horizontal line array legs. Data from the vertical array were also used independently to help determine the vertical arrival structure of the noise field for comparison with the result from the 3D calculation. The measured hydrophone data from both arrays were spectrum analyzed, and 64 beams per array heading were formed by a frequency domain beamformer[14] which creates beams non-linearly spaced in real azimuth space. Results for each array and each leg were then assessed for acceptable data quality[15]. Those data that passed the assessment were then processed with the 3D algorithm discussed above. Table 1 associates the specific measurement and processing polygons to measurement site areas.

Table 1. Measurements sites and associated polygons.

Measurement Site	Associated polygons
Site A	Polygon 7 or Polygon 17
Site D	Polygon 1 or Polygon 11
Site E	Polygon 4 or Polygon 14

Figure 4 shows the results for 100 Hz at site A (polygon 7) that were obtained from the 3D algorithm by using only the towed horizontal line array data. The upper left-hand plot in Fig. 4 is the 3D representation of the spatially averaged and temporally smoothed noise field. The vertical axis is a representation of the angular range of the vertical (or elevation) angle ϕ. Vertically up is 90 deg and vertically down is -90 deg. The horizontal axis is a representation of azimuth angle from 0 deg to 360 deg of the compass (north to north). The magnitudes of the noises that are plotted relative to the omnidirectional level in dB are given by the color bar at the lower right-hand corner of Fig. 4.

The plot in the upper right-hand corner of Fig. 4 is the estimate of the vertical directionality of the noise field represented by the noise surface plot in the upper left-hand corner. The estimates of the vertical directionality in the upper right-hand corner are plotted relative to the omnidirectional level in dB. The solid black curve represents the average levels obtained by summing the noise power along all azimuths at a given elevation in the surface plot. The curve is an estimate of what a vertical line array would have measured if it had been at approximately the same measurement location and depth as the towed array and with approximately the same temporal averaging. The black vertical dashed line is an isotropic average power reference line. Deviation of the vertical directionality curve from the isotropic reference line illustrates the degree of anisotropy of the vertical directionality curve. The other two curves in the vertical directionality plot are vertical slices across the noise surface plot showing the vertical directionality at two different azimuths. One slice (the light blue vertical curve) is where the noise has one of the many maxima near the horizontal, and the other (the pink vertical curve) is where the noise has a minima near the horizontal and maxima near ±30 deg elevation angle. The difference between the extremes in the vertical directionality curves is more than 30 dB. This difference could not be measured by either a horizontal or a vertical array separately, or combined without the 3D algorithm. Furthermore, before development of the 3D algorithm, a directionality estimate similar to the surface plot in Fig. 4 would have been possible only with data from a 2D or 3D array.

9

The plot at the bottom of Fig. 4 gives the spatially smoothed and temporally averaged 2D azimuthal directionality of the ambient noise field (solid black curve) plotted relative to the omnidirectional level in dB. This curve is obtained in a manner similar to the black curve in the vertical directionality plot, by summing the power over all vertical angles for each azimuth angle. It is this curve that most closely resembles the 2D estimates of the ambient noise field that other techniques, such as those in Refs. 6-11, attempt to generate. The black horizontal dashed line in this plot is the cylindrically isotropic average power level reference curve. Deviation from that reference curve is a measure of the anisotropy of the noise field in azimuth. The two colored dashed curves in this plot are the azimuthal directionalities (appropriately normalized) of slices at the two different elevation angles in the surface plot. The red curve is a slice at 0 deg elevation angle, and the blue curve is a slice at +30 deg elevation angle.

Summary information and some pertinent parameters have been included at the bottom right-hand corner of Fig. 4. The levels in all of the plots are relative to the omnidirectional noise level (OMNI) in dB. The frequency (FREQ) is 100.0 Hz, and the standard deviation of the estimate (STDEV) is 5.90 dB. This is a relatively low standard deviation and indicates that the results can be accepted with a high degree of confidence.

One way of evaluating the 3D algorithm is to compare it with the 2D algorithm,[10] which has enjoyed wide acceptance for many years. The comparison can be done on the basis of the directionality that is obtained when the noise is summed over all elevation angles of the surface plots (solid black curve at the lower left-hand corner of Fig. 4). This process eliminates the vertical dimension, and produces a 2D noise directionality curve that can be directly compared to the corresponding curve produced by the 2D algorithm. The comparison is made simple if this curve is presented in a polar plot.

Figure 5 compares the horizontal directionalities for 100 Hz at site A, obtained from the previous 2D algorithm[10] (thick curve) and from the 3D algorithm (thin curve). The omnidirectional levels obtained from the directionality estimate differed by no more than a fraction of a decibel. However, there are significant differences between the two estimates along some azimuths, and there are remarkably good agreements between the two estimates along large regions of azimuth. There are four regions of azimuth where the 3D estimate is much lower than the 2D estimate (i.e., near 30 deg, 120 deg, 180 deg, and 225 deg). On the other hand, the 2D algorithm gave a lower estimate along three small regions of azimuth (i.e., near 305 deg, 330 deg, and 355 deg). It is not possible from these results, or from similar results for the other sites, to quantify the magnitude of the

agreement and disagreement in a statistically significant manner. However, an "eye ball" evaluation suggests that the 2D and the 3D algorithms generally produce similar 2D results. The 3D algorithm can be expected to achieve lower levels in some areas of azimuth where the 2D algorithm does not, because the 3D algorithm can partition the noise more realistically, in three dimensions, than the 2D algorithm can partition the noise in two dimensions. This is especially true where the noise level is actually lower. After all, noise is a three dimensional quantity, and the 3D algorithm is more closely tied to a realistic 3D arrival structure, and to the 3D response pattern of the array. Hence, when there are disagreements between the two algorithms, the 3D estimate should have the higher level of confidence associated with it. The limited number of simulations that have been performed tend to support this contention.

The ambient noise 3D directionality surface plot in Fig. 4 is interesting for several reasons. First, both the left-right and up-down ambiguities have been resolved. Second, although the ambient noise, for the most part, is concentrated within about 30 deg of the horizontal, there are azimuths where most of the noise does not arrive at or near 0 deg elevation angle, but arrives in concentrations around ±30 deg elevation angles. There are also azimuths where very little noise arrives, regardless of elevation angle. Third, the algorithm (and plot) provides an estimate of the 3D noise field obtained from data acquired by a towed horizontal line array, an asset that is common to the inventories of many navies, as well as research establishments, or can be rented from the petroleum exploration community. Furthermore, the plot provides the results from which the performance of much more complex and expensive multi-dimensional arrays can be estimated. Finally, the results provide insight into the 3D arrival structure of the noise field that must otherwise come from measurements by multi-dimensional arrays. At the present time, measurements with multi-dimensional arrays are not a realistic expectation. Given the current projections for undersea research, this may not be a reasonable expectation for many years to come.

Figure 6 shows the results for 100 Hz at site A, obtained from the 3D algorithm using data from both the towed horizontal array and the vertical line array. Comparison of the results in Figs. 4 and 6 show that the inclusion of the vertical array data at this site had a tendency to concentrate the noise more toward 0 deg elevation angle. In all other respects, the two figures are very similar.

Specific features of the noise shown in Fig. 6 can be correlated to the noise source distributions and the acoustic propagation environment. The noise arriving near 0 deg elevation angle, along an azimuth of approximately 150 deg, comes from the major

northern access for coastal steamers to the port of Bodø, Norway. Noise generated closer to Bodø, and at the southern access to Bodø, is blocked by Landegode and other small islands, as well as the relatively shallow bathymetry in these areas (160 deg to 185 deg azimuth angles). The noise arriving near 0 deg elevation angle from azimuths between approximately 185 deg to 245 deg is most likely distant shipping noise propagating up and into the fjørd from the Norwegian Sea. Along azimuths of 245 deg to 330 deg, the noise is arriving from the lower Lofoten Islands. Propagation conditions along these azimuths are not conducive to long range propagation, or down-slope conversion of the noise to vertical arrival angles near 0 deg. The bathymetry in this area, when compared to the bathymetry along the southern side of the Vestfjørd, has a gentler slope, and is not expected to be as highly reflective (see Fig. 3). Furthermore, these paths are along the slope, which gives rise to a propagation path which curves (seaward) away from site A. Thus, only nearby shipping can contribute from these azimuths. This may in part explain the reason for the noise concentrations at ±20 deg elevation angles, rather than near 0 deg elevation angle. The noise arriving near 0 deg elevation angle, along azimuths between approximately 330 deg and 25 deg, comes from the direction of the upper Lofoten Islands and the routes for coastal steamers in that area. The azimuths between 25 deg and 60 deg include up-slope propagation paths from further up the Vestfjørd.

Figure 7 shows the results for 48 Hz at site A, obtained from the 3D algorithm using data from both the towed horizontal array and the vertical line array. The array used to collect the data reported herein had a nominal design frequency of 375 Hz. This means that, of the 64 beams produced by the beamformer, at most nine beams are real for the lower frequency data (50 Hz and below), which leads to a slightly smoother 3D noise estimate. There are several regions of azimuth along which the noise arrives near the horizontal. In addition, there is one larger region, perhaps an artifact, along which the noise arrives from very high vertical arrival angles. This particular region is large most likely because of the width of the endfire beams of the vertical array. Regardless, the 48 Hz results can be used to gather information about the lower frequency propagation conditions. Interpreted in this light, the 48 Hz results in Fig. 7 correspond well with the results for 100 Hz (Fig. 6) and support the conclusions made about the propagation in the 100 Hz discussion above.

Similar observations can be made for the 350 Hz results, which can be found in Fig. A1 in the Appendix.

12

Figure 8 illustrates the results for 100 Hz at site D (polygon 1), which were obtained from the 3D algorithm using data from both the towed horizontal array and the vertical line array. Site D is outside the Vestfjørd, to the north and west of the Lofoten Islands, on the relatively shallow Norwegian continental shelf. It is evident from Fig. 8 that the noise at site D is concentrated between vertical arrival angles of ±30 deg. Similar to site A in Fig. 6, there are azimuths which have the noise concentrated near 0 deg elevation angle, azimuths which have noise concentrations at high vertical angles, and azimuths which have very little noise at any vertical arrival angle. The broad region of noise around North (345 deg - 25 deg) is believed to be due to ships in the general direction of Spitsbergen and the Svalbard Islands. The quiet region between 25 deg and 45 deg can be attributed to adverse propagation along a steep slope. As discussed earlier, this type of propagation condition can curve the noise away from the measurement site, and reduce the noise considerably along affected azimuths. The noise arriving along azimuths between 45 deg and 110 deg is from the direction of the northern shelf down to the Vesterålsfjørd. This region includes shipping accesses to the ports of Tromsø and Harstad, and includes routes for coastal steamers. The region of noise from azimuths between 110 deg to 160 deg is in the direction of the seaward side of the upper Lofoten Islands down to the Moskenestraumen. This area has a very steep downward sloping bottom, which can convert the vertical arrival angles of the acoustic energy into elevation angles that are very near to 0 deg elevation angle. The noise along azimuths from 160 deg to 225 deg is concentrated at vertical arrival angles close to ±20 deg. This feature is indicative of propagation conditions that do not encourage conversion of energy from higher vertical arrival angles into lower elevation angles. Indeed, the bathymetry along these azimuths rarely goes below 200 m north of the mouth of the Vestfjørd. In addition, this region is dominated near site D by a claystone low loss bottom. The azimuths between 225 deg and 315 deg receive noise near 0 deg elevation angle, which is consistent with distant shipping. Finally, it is believed that the quiet area along azimuths between 315 deg and 345 deg occurs because no distant shipping is expected at such high latitudes.

The site D results for 48 Hz and 350 Hz for can be found in Figs. A2 and A3 in the Appendix.

Figure 9 illustrates the results for 100 Hz at site E (polygon 4), which were obtained from the 3D algorithm by using data from both the towed horizontal array and the vertical line array. In a manner similar to site D (Fig. 8), the noise is concentrated between ±20 deg vertical arrival angles. Furthermore, it is evident that the noise is more highly concentrated near the horizontal than at the other two sites. Again, the region of azimuths

13

near north (355 deg to 30 deg) are toward the general direction of Spitsbergen and the Svalbard Islands. The relatively quiet region between 30 deg and 45 deg azimuth is where distant propagation must proceed along a steep slope, such that only nearby shipping can be a major contributor. The noise arriving from azimuths between 45 deg and 90 deg comes from the direction of the northern shelf down to the Moskenestraumen. This region includes shipping accesses to the ports of Tromsø and Harstad, routes for coastal steamers, and the seaward side of the upper Lofoten Islands. As noted above, this area includes regions with a very steep downward sloping bottom, which can convert acoustic energy into elevation angles that are close to 0 deg. The noise between azimuths of 90 deg to 135 deg comes from the lower Lofoten Islands, and propagates over the above mentioned claystone area. The azimuths between 135 deg and 170 deg include noise contributions from nearby shipping from the access to the Vestfjørd around the end of the Lofoten Islands, which gives rise to the noise at "high" elevation angles. This region also includes noise from shipping along the Norwegian coast that is characterized by a hard bottom and steep slopes. As discussed earlier, this allows for down-slope conversion of the acoustic energy into elevation angles near 0 deg. Distant shipping is the most probable contributor to the noise between the azimuths of 170 deg and 290 deg.

Figure 10 illustrates the results for 150 Hz at site E (polygon 4), which were obtained from the 3D algorithm by using data from both the towed horizontal array and the vertical line array. Since this is the only result obtained at 150 Hz, it is being presented here. As can be seen from a comparison of Figs. 9 and 10, there is little difference between the 150 Hz results and the 100 Hz results. In general, the noise at 150 Hz tends to arrive at slightly higher elevation angles and to be more dispersed than the 100 Hz results.

The site E results for 48 Hz and 350 Hz are given in Figs. A4 and A5 of the Appendix.

OPTIMUM ARRAY HEADING SELECTION

Towed array performance in shallow water areas is highly influenced by the extreme temporal and spatial variability of the shallow water noise environment. The spatial variability includes physical properties (bottom type, subbottom structure, etc.), topographical features, and shipping distributions. The temporal variability includes internal waves, kinematical fluctuations, source level fluctuations, and seasonal variations. It is these fluctuations and variabilities that can be exploited to enhance the signal-to-noise

14

ratio (S/N) gains achieved by a towed horizontal line array in shallow water. Given the complexity of these fluctuations and variabilities, the task of processing, manipulating, and implementing this knowledge in a reasonable time frame (near real-time) is monumental. The solution is to automate/computerize as much of the task as possible to aid the operator in exploiting the shallow water environment and maximizing the performance of the towed horizontal line array. Such an automated tool is called a tactical decision aid. An example of a tactical decision aid, the Array Heading Rose (AHR), is illustrated in Fig. 11.

The Array Heading Rose is a tactical decision aid that can be used to select the heading of the array, or the course of the towship, that will align the unique ambiguous beam patterns of the towed array with the horizontal directionality of the ambient noise field in such a way that the S/N can be maximized. The AHR presents the S/N in decibels relative to broadside performance as a function of the array heading and search sector. The best heading is the one that gives maximum S/N within the navigational constraints of the towship for the search sector of interest. The AHR can also be used to determine which array headings to avoid.

Array Heading Rose results such as that in Figure 11 are for 30 deg wide search sectors centered on bearings of 45 deg (upper left AHR plot), 135 deg (upper right AHR plot), 225 deg (lower left AHR plot), and 315 deg (lower right AHR plot). The AHR plots in Fig. 11 are for 48 Hz at site E. The radial distance of a point on the AHR curve (blue curve) in Fig. 11 corresponds to the S/N level improvement in performance of a towed line array, when the array is on a heading that corresponds to the azimuth angle of the point on the curve. The S/N performance improvement is relative to that which would be achieved if the beams near broadside were in the detection sector instead of those near broadside. In this case of the AHR for a search sector centered at 45 deg (upper right AHR in Fig. 11), an array heading of approximately 160 or 340 deg would provide a S/N improvement of 10 dB over broadside performance for finding sources in the indicated search sector. The AHR plot is symmetric through the origin (repeats after 180 deg) because of the forward-aft symmetry of the line array. In the event that the heading of maximum S/N improvement cannot be used (i.e., for geographical constraints or adverse seas for that ship's course), the AHR permits the selection of alternate headings, and predicts the improvements or degradations in S/N that would result.

The site E AHR plots for 100 Hz, 150 Hz, and 350 Hz are given in Figs. A6, A7, and A8 of the Appendix. The AHR plots for site A and site D can be found in Fig. A9 through Fig. A12 and Fig. A13 through Fig. A16 of the Appendix, respectively.

15

The Array Heading Rose concept for a search sector at a single azimuth can be generalized to include all possible (i.e., 360) search sector center azimuths. This is done by calculating a separate AHR for a search sector centered at each degree of azimuth. The Array Heading Rose results are then plotted along a horizontal line that has a vertical position on a Cartesian coordinate system (rectangular plot) that corresponds to the search sector center azimuth. Three hundred and sixty such AHRs are thus calculated. Since the AHR is symmetric through the origin (repeats after 180 deg), the AHR can be plotted for azimuth angles from 1 deg to 180 deg with no loss of information. The result is an Array Heading Surface (AHS). Array Heading Surfaces for 48, 100, and 150 Hz for site A have been combined in the sample illustrated in Fig. 12. Such a presentation facilitates optimizing the array heading for all three frequencies simultaneously.

The superimposed horizontal directionality plots (noise roses) in the upper right-hand corner of Fig. 12 are the noise roses for which the AHS plots in this figure were generated. The vertical axis gives the center azimuth of the search sector (30 deg wide in this example), and the array heading is along the horizontal axis (0 to 360 possible). When searching for a target in a particular direction (i.e., 45 deg), one reads across the plot from that sector direction and finds the maximum level. The array heading corresponding to this location on the plot is the best heading for the array. The plotted level is the S/N gain improvement over broadside performance that could be expected in the noise field for which the plot was generated. Black indicates gains above the color scale, and magenta indicates gains (losses) below the color scale. This plot has a great deal of utility as a tactical decision aid when there is no prior intelligence to predetermine a search sector. Sector directions could be chosen from the plot to maximize the S/N gain improvement, or to maintain it at a relatively high level while going on various headings to search an area.

The AHS plots in Fig. 12 clearly show a range of sectors from about 30 deg to 60 deg wherein the performance improvement exceeds 8 dB, depending upon array heading and frequency. The AHS is relatively easy and straight forward to use. One simply determines the center bearing for the search sector, follows that bearing across the AHS to a maximum or acceptable level of improvement, and then reads off the corresponding array heading for that point on the AHS.

Additional AHS plots for site A, as well as all the AHS plots for site D and site E can be found in Fig. A17 through Fig. A21 of the appendix.

16

OBSERVATIONS AND CONCLUSIONS

The pseudo-stationary ambient noise field 3D arrival structure can be significantly different and more complex than either its vertical or its horizontal directionality. Both are significantly degraded by the spatial smoothing that results from the 2D nature of the analysis. However, the 3D nature of the method presented herein is able to resolve the arrival structure of the noise simultaneously in the vertical angle and the horizontal angle, and provide a more credible estimate of the noise field arrival structure. In doing so, the regions of low level noise are well identified and separated in elevation and azimuth angles from the regions of high level noise. The resulting 3D noise field arrival structure estimates can be used to predict the noise response of any array, whether it is a relatively simple vertical or horizontal line array, a more complicated tilted line array, a planar array, or even a multi-dimensional array.

The pseudo-stationary ambient noise field 3D arrival structure can also be used in conjunction with the propagation environment to gain insight into the source distributions and propagation mechanisms that existed during the measurement. Such analysis techniques were performed for three sites in the Vestfjørd, Norway, area at 48, 100, and 350 Hz to identify important propagation parameters and features. Inside the Vestfjørd, site A was not exposed to distant shipping from most azimuths, but did receive noise near 0 deg elevation angle on many azimuths. This was most likely due to environmental conditions which supported down-slope conversion of the acoustic energy into vertical angles closer to 0 deg elevation angle. The noises at site D and site E were more concentrated near 0 deg elevation angle and could be associated with distant shipping. At both sites, however, the same down-slope conversion conditions existed to allow for noise arriving near 0 deg elevation angle from directions in which distant shipping was not possible. For all three sites, there were situations in which the distant shipping noise contributions did not appear in the 3D estimate of the noise field, even though distant ships were known to be present. These cases were from azimuths that were along, rather than across, a steep slope that would cause the sound propagation paths to curve away from the measurement site and cause an absence of noise near 0 deg elevation angle.

It is possible, at two of the measurement sites, to achieve significant improvements in the S/N (i.e., sometimes greater than 9 dB), by using the Array Heading Roses (AHR) and Array Heading Surfaces (AHS) to aid in selecting the best array heading for a particular search sector.

17

ACKNOWLEDGMENTS

REFERENCES

1. R. J. Urick, "Ambient Noise In The Sea," Undersea Warfare Technology Office, Naval Sea Systems Command, 1984.

2. P. C. Etter, <u>Underwater Acoustic Modeling</u>, Elsevier Applied Science, New York, NY, 1991, Chap. 7.

3. F. D. Tappert, "The Parabolic Approximation Method," in Wave Propagation and Underwater Acoustics, edited by J. B. Keller and J. S. Papadakis, Lecture Notes in Physics, Vol. 70 (Springer, New York, 1977).

4. P. D. Koenig, "Transient Response of Multidimensional Arrays," Naval Underwater Systems Center Technical Report, TR 7193, Jun. 1984.

5. V. C. Anderson, "Nonstationary and nonuniform oceanic background in a high-gain acoustic array," J. Acoust. Soc. Am., Vol. 67, No. 4, Apr. 1982, pp. 1170-1179.

6. A. H. Nuttall, "Estimation of Noise Directionality Spectrum," Naval Underwater Systems Center Technical Report, TR 4345, Sep. 1972.

7. A. H. Nuttall, "Resolving the Directional Ambiguities of a Line Array of Hydrophones," Naval Underwater Systems Center Technical Report, TR 4385, Sep. 1972.

8. J. H. Wilson, "Ambient-noise horizontal directionality measurements with linear arrays," J. Acoust. Soc. Am. 60, pp. 955-960, 1976.

9. E. M. Wilson, "Directional Noise Measurements with Line Arrays," Admiralty Research Laboratory, Teddington, Middlesex, Rep. No. ARL/M/N16, Jun. 1973.

10. R. A. Wagstaff, "Iterative technique for ambient-noise horizontal-directionality estimation from towed line-array data," J. Acoust. Soc. Am. 63, No. 3, pp. 863-869, 1978.

11. R. A. Wagstaff, "Horizontal Directionality estimation considering array tilt and noise field vertical arrival structure," J. Acoust. Soc. Am., pp. 1287-1294, 1980.

12. ROCKY ROAD Operation Order (CINCEASTLANT CHEL 4335/7 Ops dated 30 April 1993)

13. J. C. Scott, "Operation ROCKY ROAD. Chief Scientist's Annual Report for 1992," DRA TM(CUCS1)93141 (A/c No. 86750), May 1993

14. J. R. Williams, "Fast Beam-Forming Algorithm," J. Acoust. Soc. Amer. Vol. 44, pp. 1454-1455, 1968.

15. R. A. Wagstaff, "A Computerized System for Assessing Towed Array Sonar Functionality and Detecting Faults," IEEE J. Ocean. Eng., Vol. 18, No. 4, Oct. 1993.

16. R. A. Wagstaff and J. Newcomb, "3D noise field directionality estimation from single-line towed array data," J. Acoust. Soc. Amer. (submitted for publication).

a) "ENDFIRE" BEAM

b) BROADSIDE BEAM

0.0003   SCALE   1.0000

c) BROADSIDE BEAM, 30° TILT

d) 56° BEAM, 30° TILT
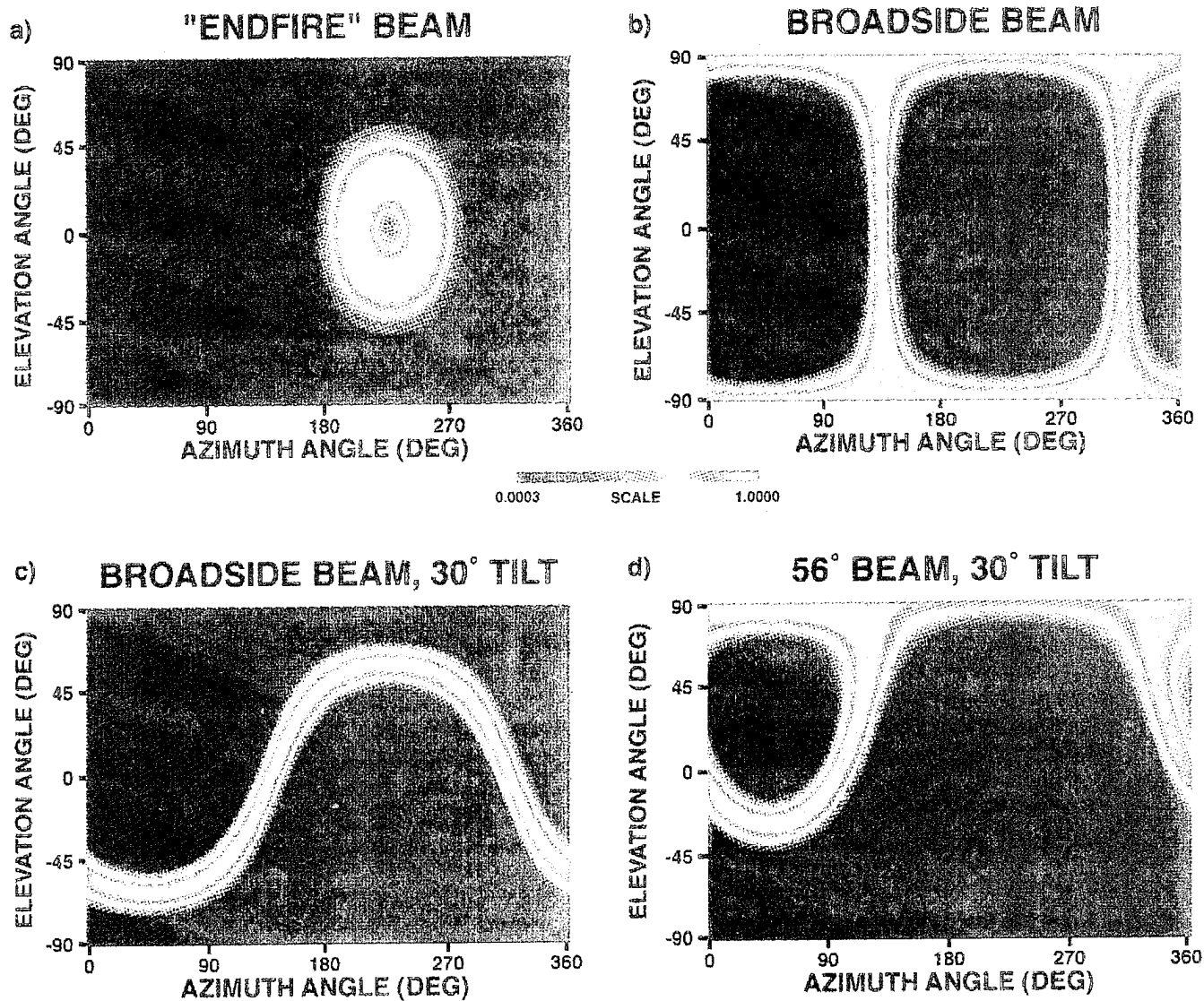
Figure 1   Three dimensional beam response patterns for a horizontal line array with no
tilt (plates a and b) and with 30° tilt (plates c and d).

20

θ   AZIMUTH ANGLE
φ   VERTICAL ANGLE
α   ARRAY TILT ANGLE
β   CONICAL ANGLE
β_s STEERING ANGLE
BW   BEAMWIDTH
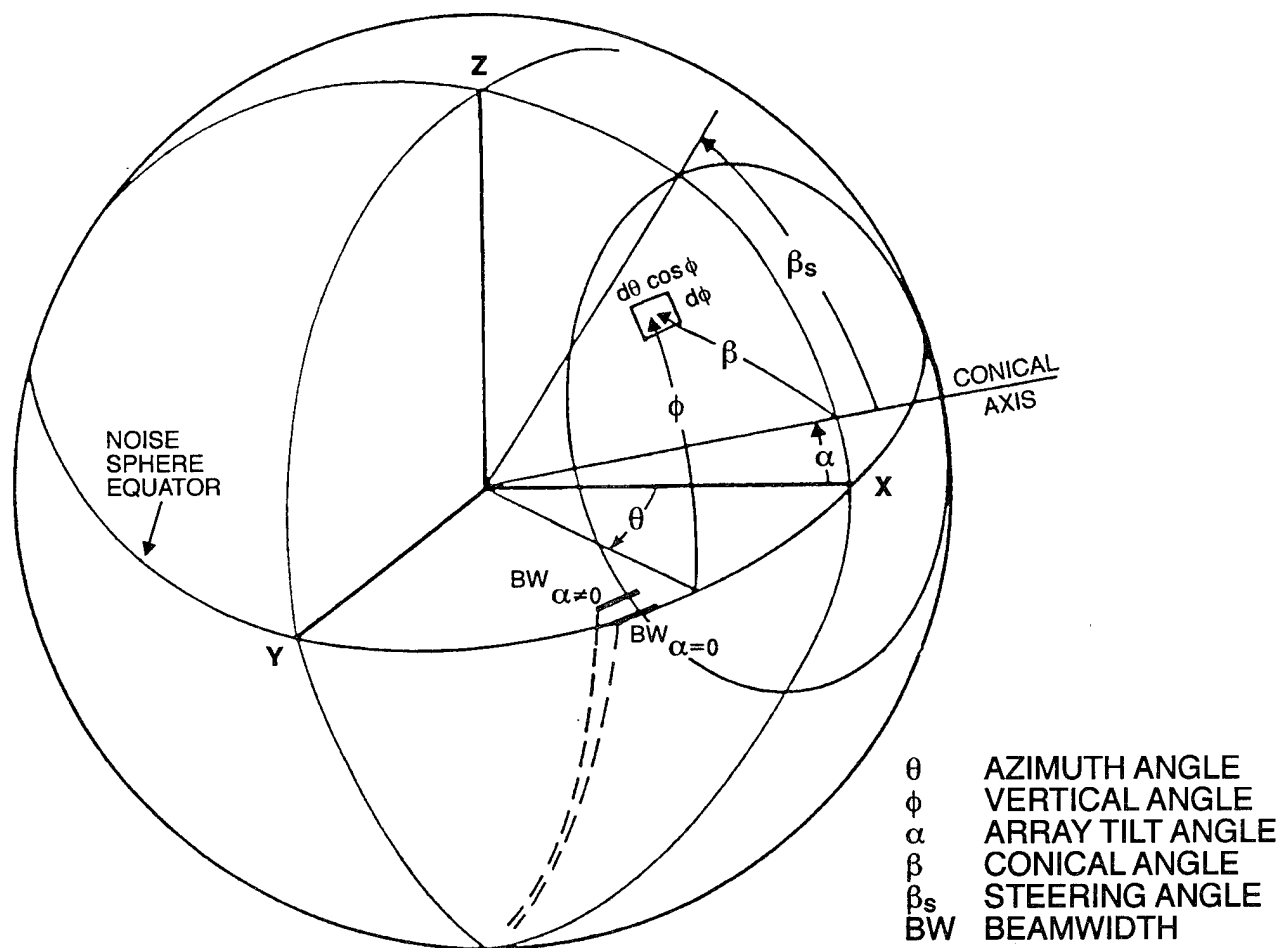
Figure 2   Coordinate system representation.

21

Figure 3　Bathymetric map of the Vestfjørd area.

22
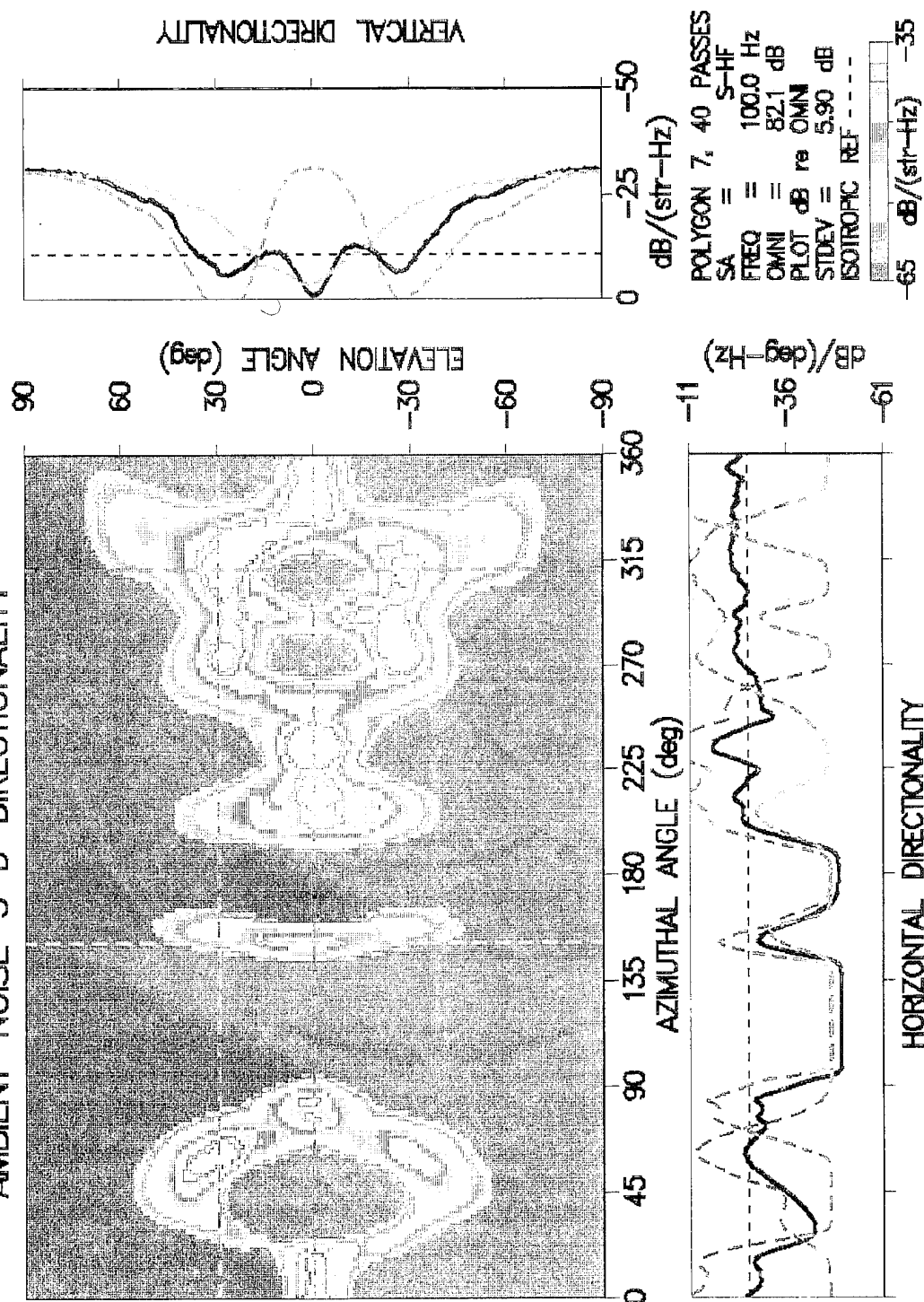
Figure 4   Ambient noise 3D directionality (top left) at site A with the corresponding 2D horizontal directionality (bottom) and vertical directionality (top right). Dashed curves correspond to cuts across the surface plot. Only data from a towed line array were used.

23

HORIZONTAL DIRECTIONALITY
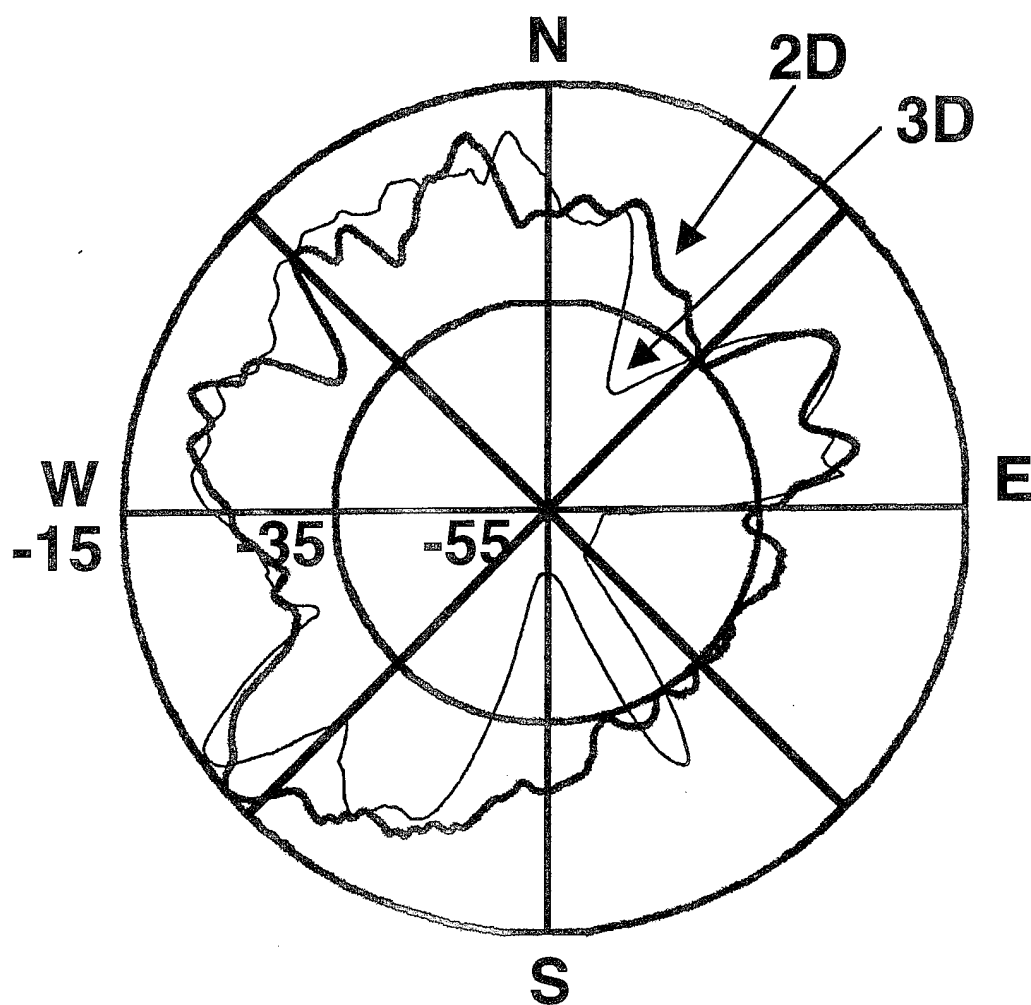
Figure 5   Ambient noise 2D directionalities for 100 Hz at site A obtained from the 3D
algorithm (thin curve) and from the 2D algorithm from reference 10. Noise
levels are relative to the per-horizontal-degree omnidirectional reference curve
(dashed circle).

AMBIENT NOISE 3-D DIRECTIONALITY

VERTICAL DIRECTIONALITY

POLYGON 7, 40 PASSES
SA = S-HF
FREQ = 100.0 Hz
OMNI = 83.7 dB
PLOT dB re OMNI
STDEV = 5.21 dB
ISOTROPIC REF ----

dB/(str-Hz)

ELEVATION ANGLE (deg)

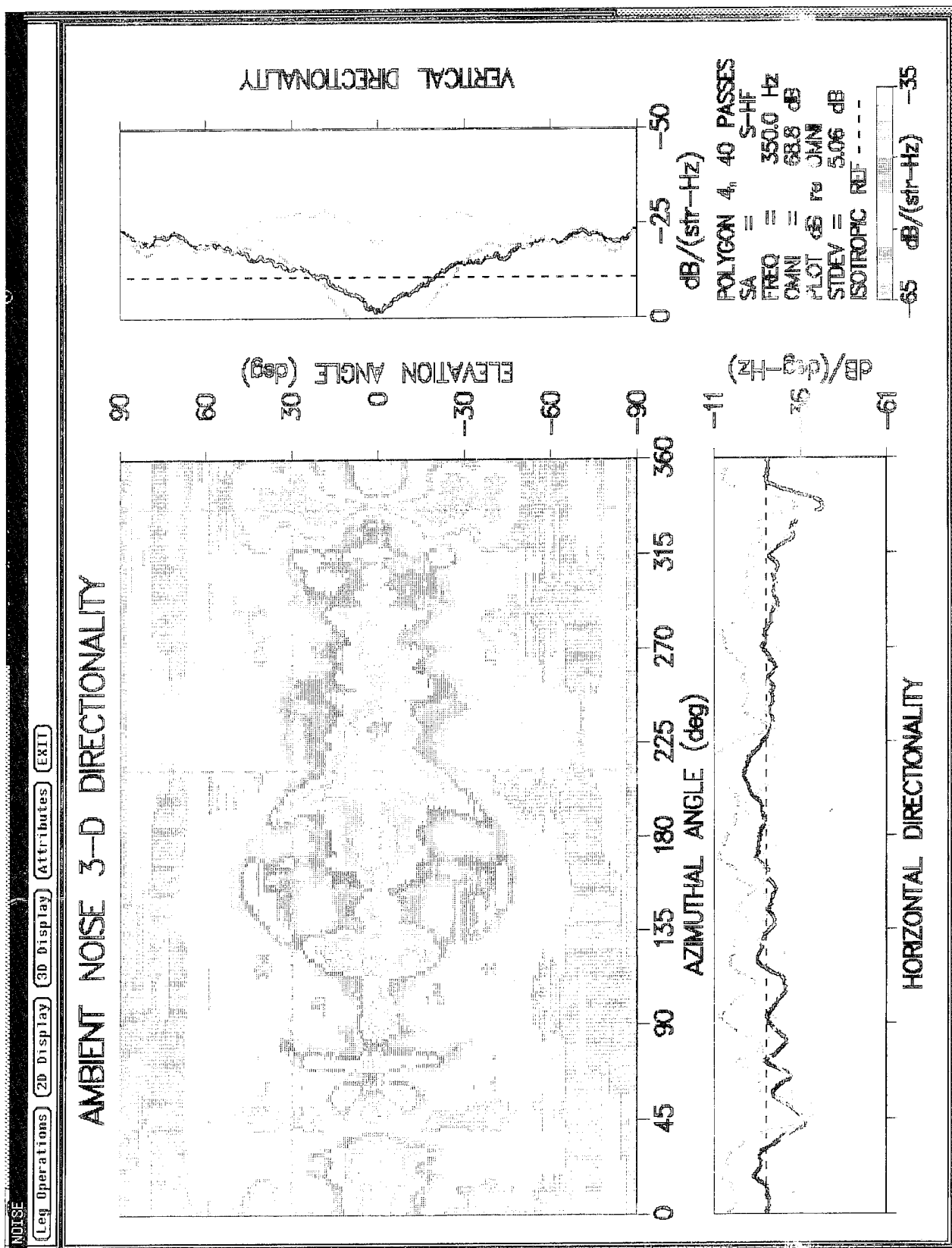AZIMUTHAL ANGLE (deg)

dB/(deg-Hz)

HORIZONTAL DIRECTIONALITY
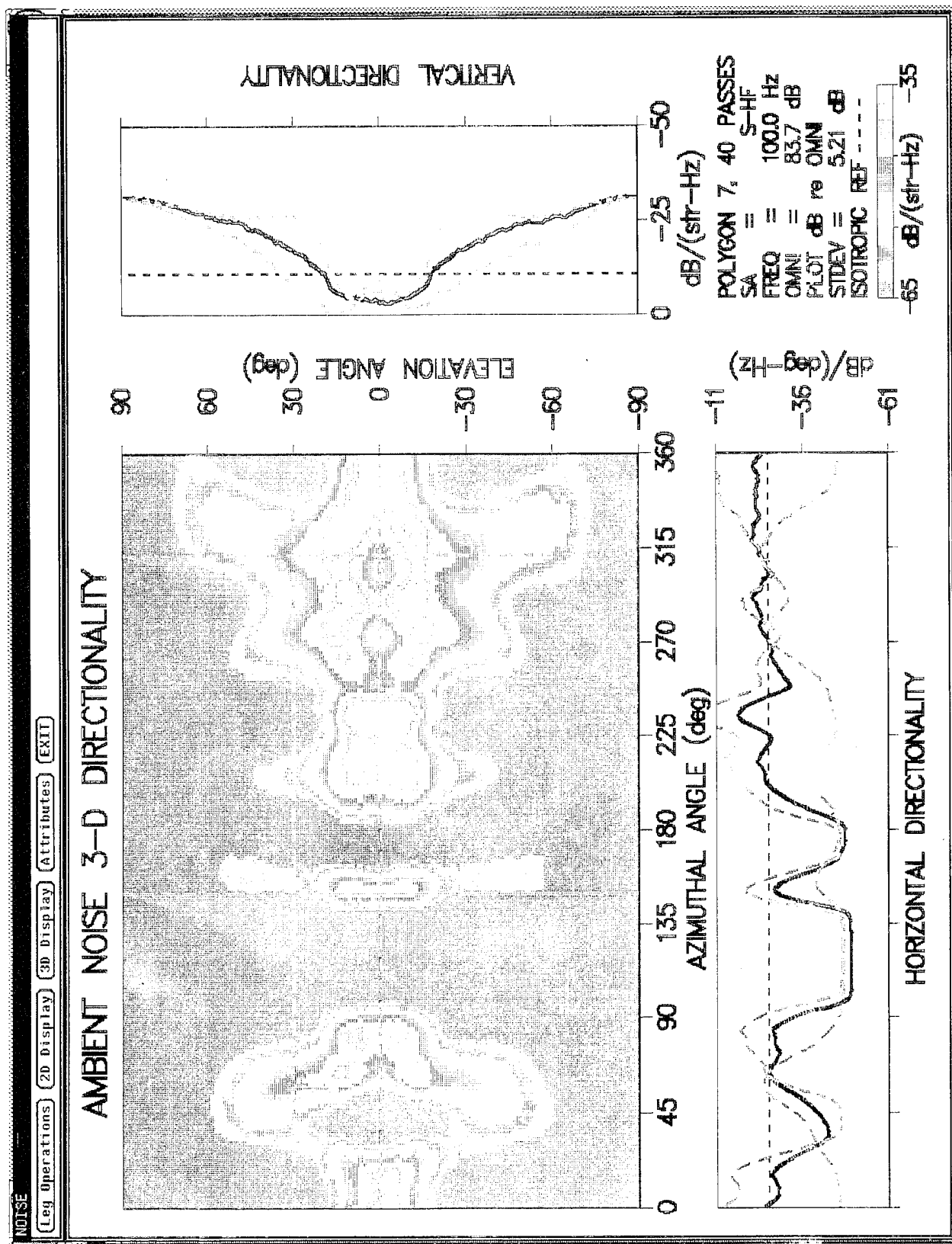
Figure 6   Ambient noise 3D directionality plot for 100 Hz at site A using data from both towed line and vertical line arrays were used.

Figure 7   Ambient noise 3D directionality plot for 48 Hz at site A using data from both towed line and vertical line arrays were used.
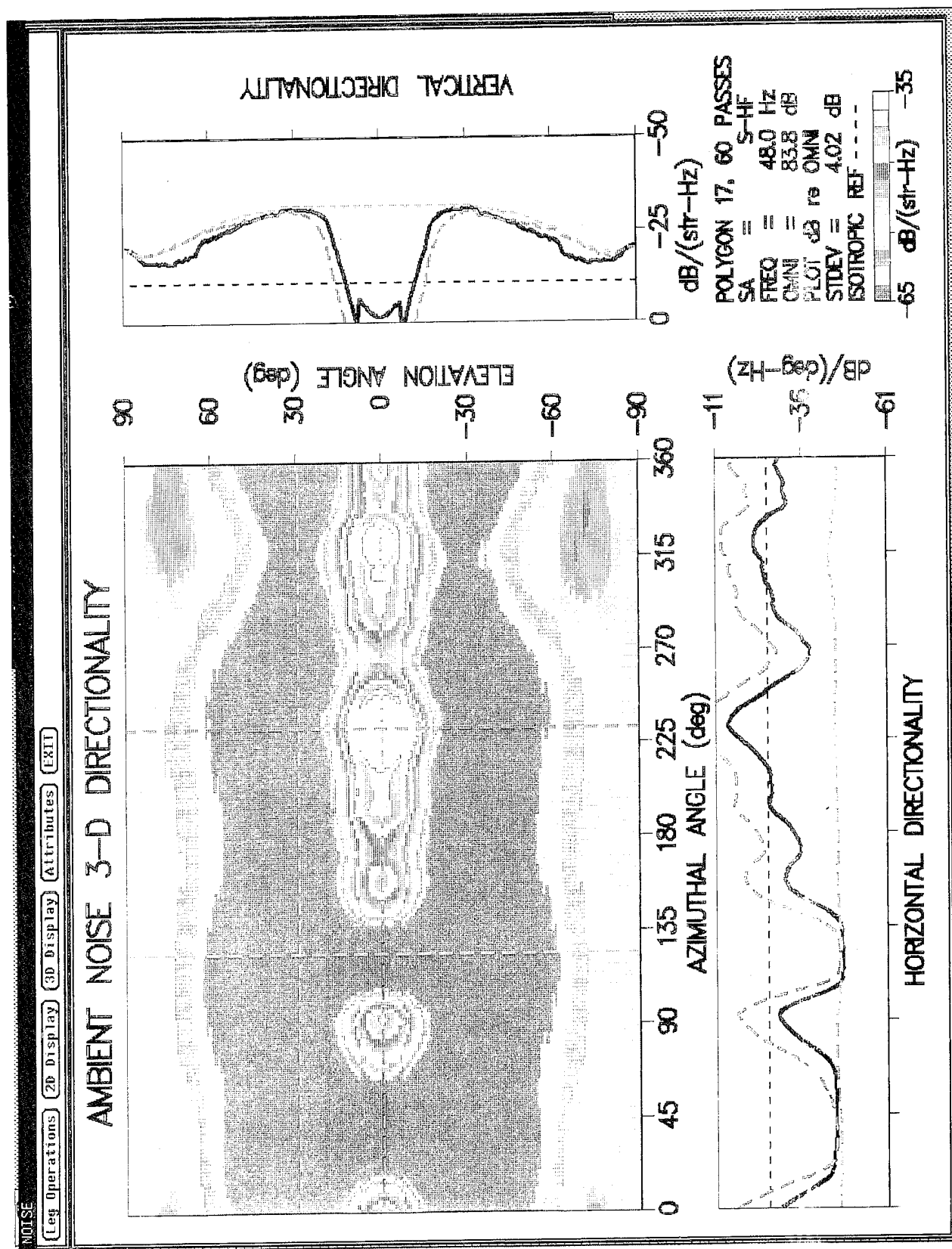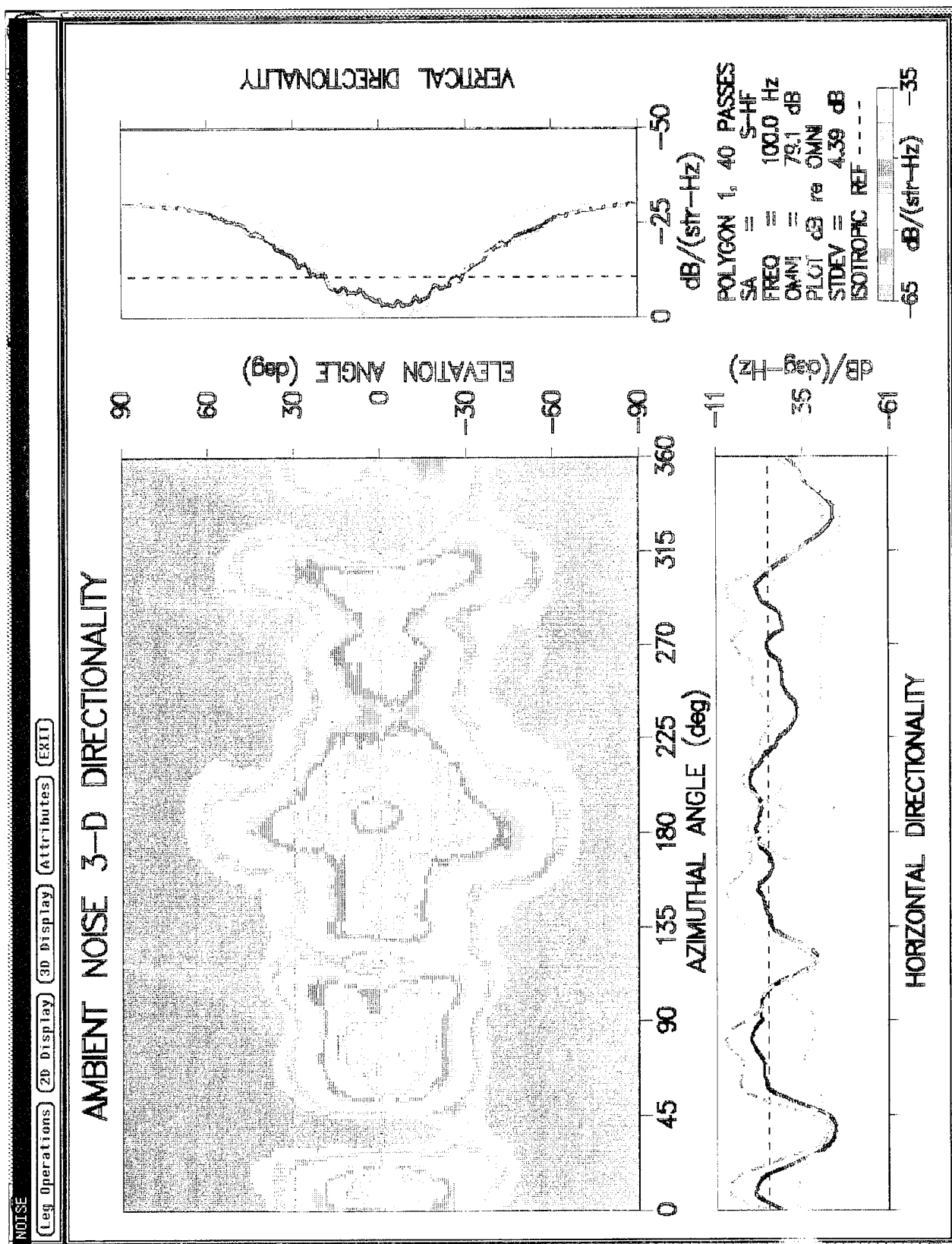
Figure 8   Ambient noise 3D directionality plot for 100 Hz at site D using data from both towed line and vertical line arrays were used.
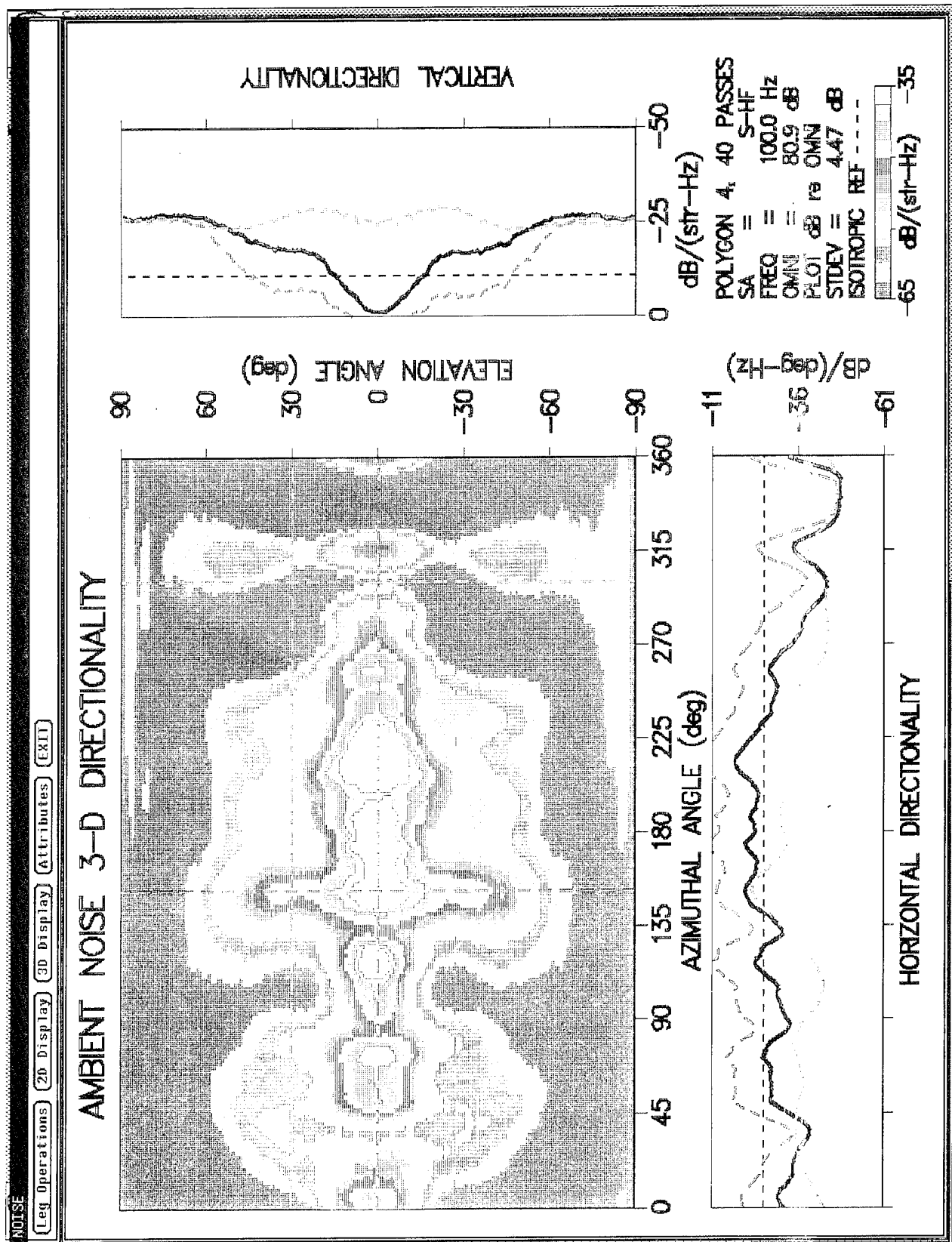
Figure 9   Ambient noise 3D directionality plot for 100 Hz at site E using data from both towed line and vertical line arrays were used.
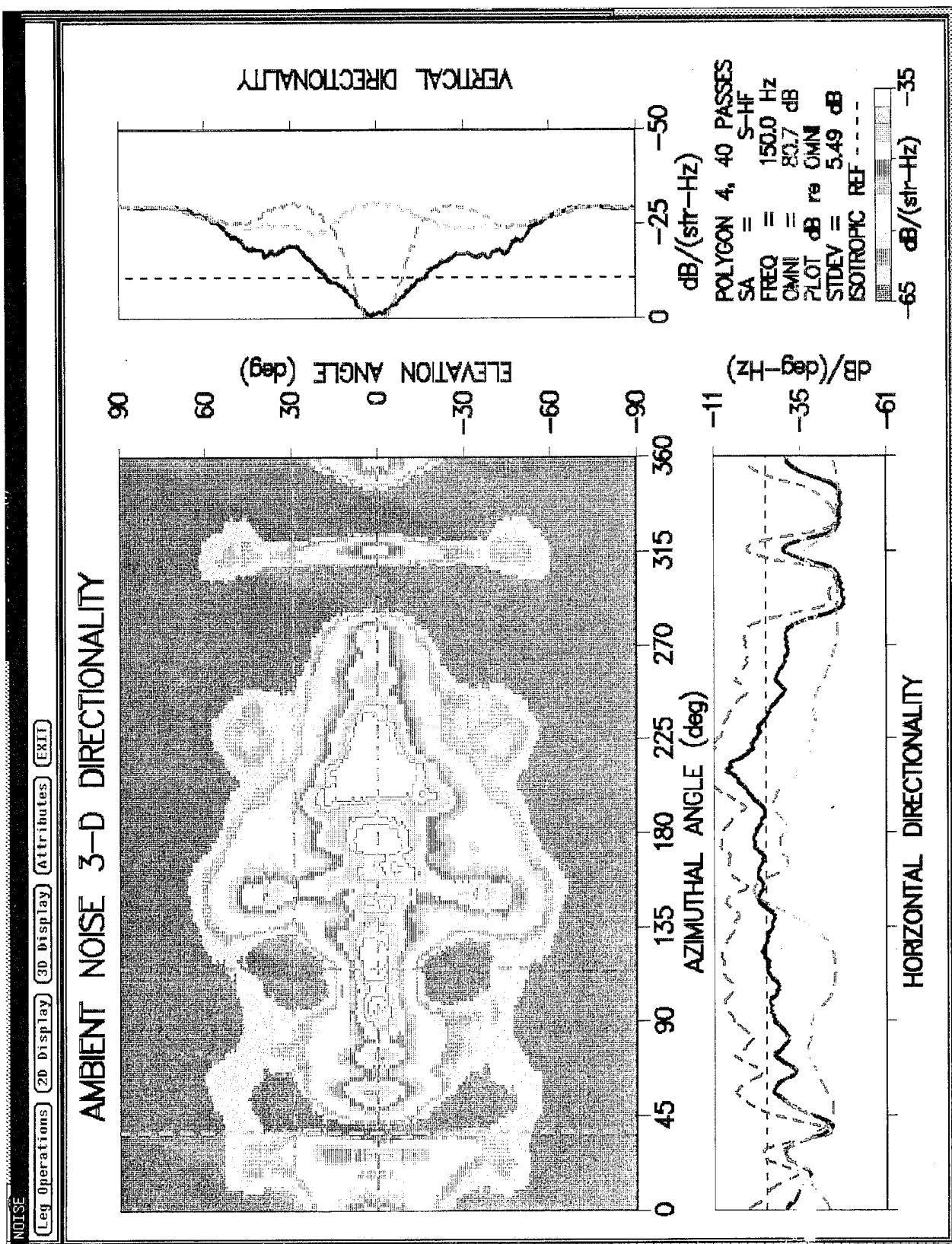
Figure 10 Ambient noise 3D directionality plot for 150 Hz at site E using data from both towed line and vertical line arrays were used.
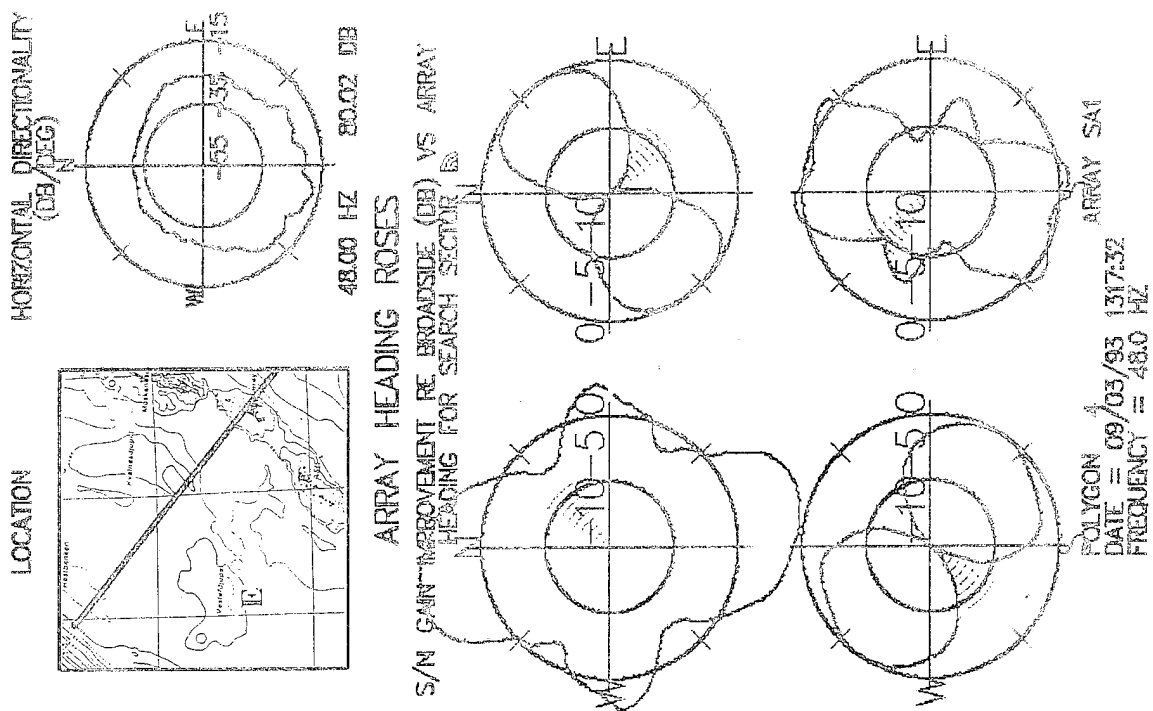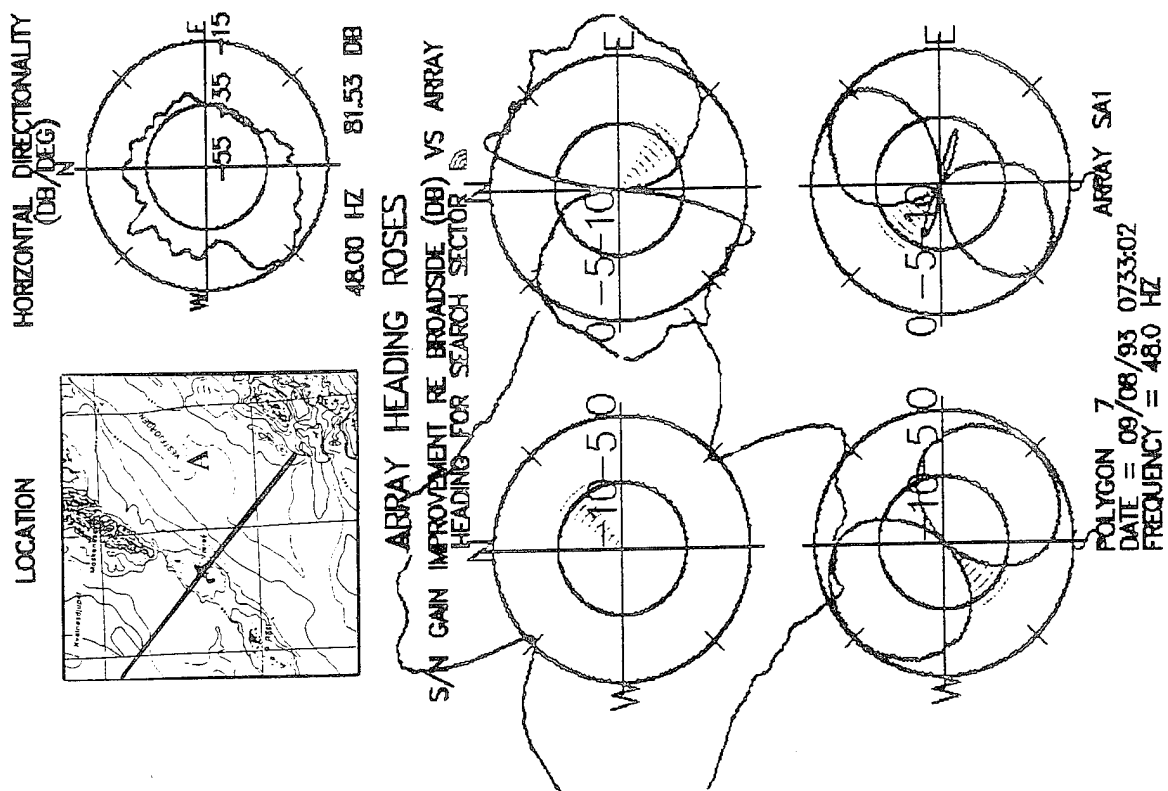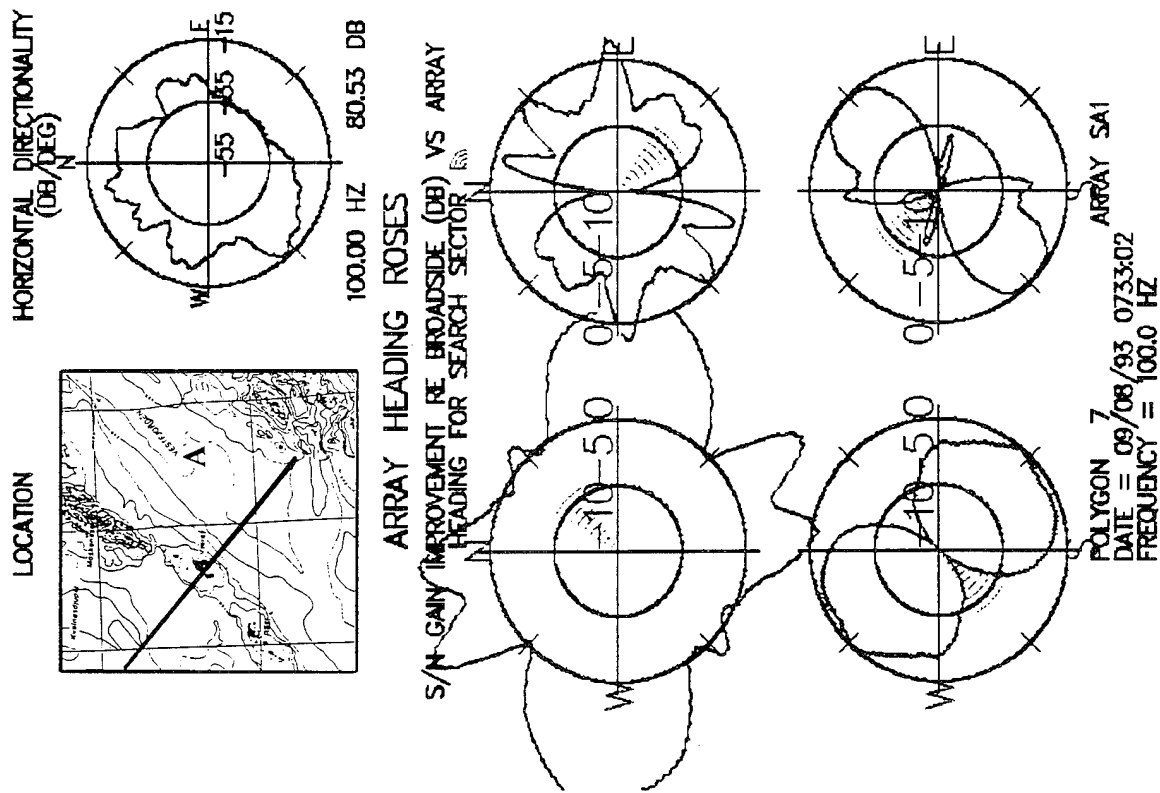
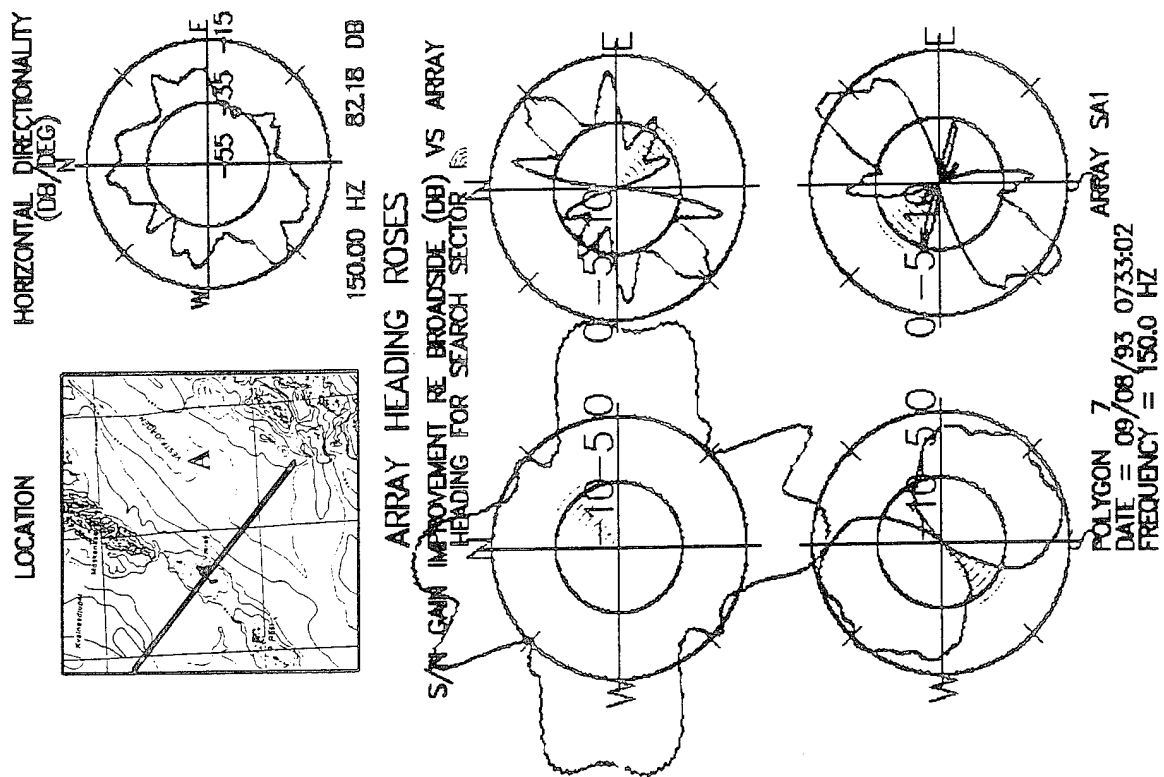Figure 11 Array Heading Rose plots, corresponding noise rose, and geographic location for site E for 48 Hz.

Figure 12 Array Heading Surfaces for 48 Hz (left), 100 Hz (middle), and 150 Hz (right), at site A with corresponding noise roses (top right hand corner). The omnidirectional levels are included opposite the frequency beneath the noise roses.

31
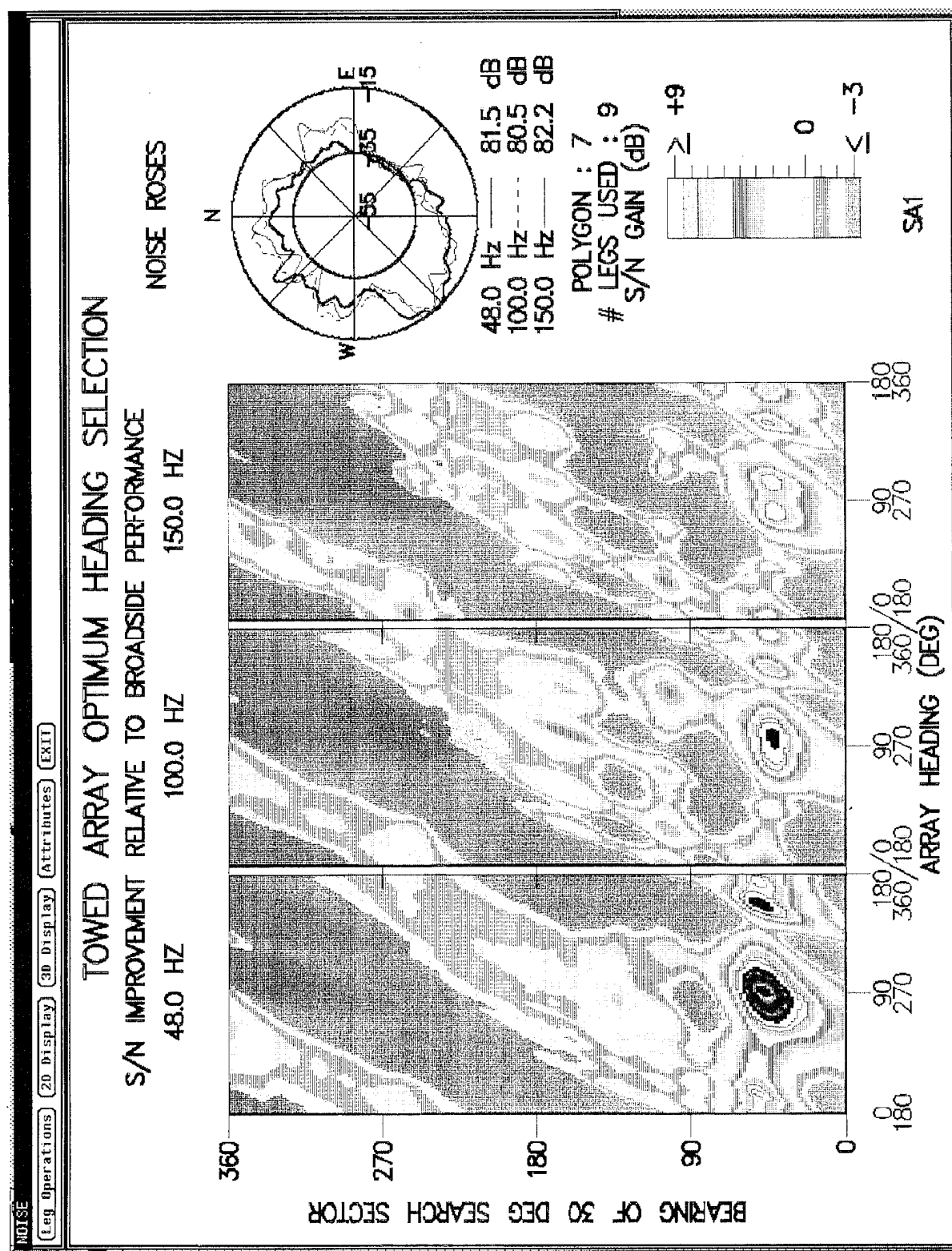
APPENDIX

ADDITIONAL PLOTS OF ANALYSIS PRODUCTS
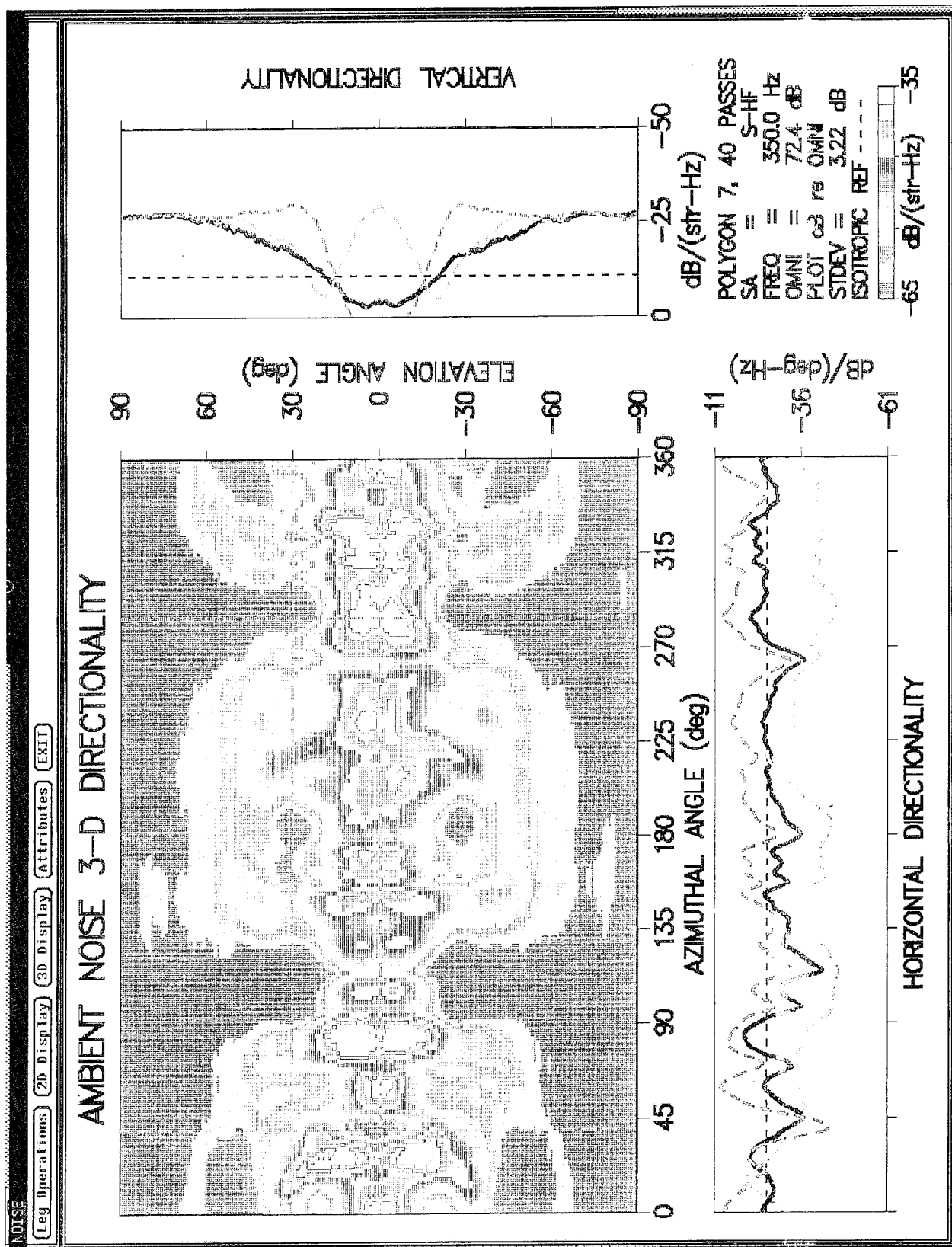
Figure A1   Ambient noise 3D directionality plot for 350 Hz at site A using data from both towed line and vertical line arrays were used.
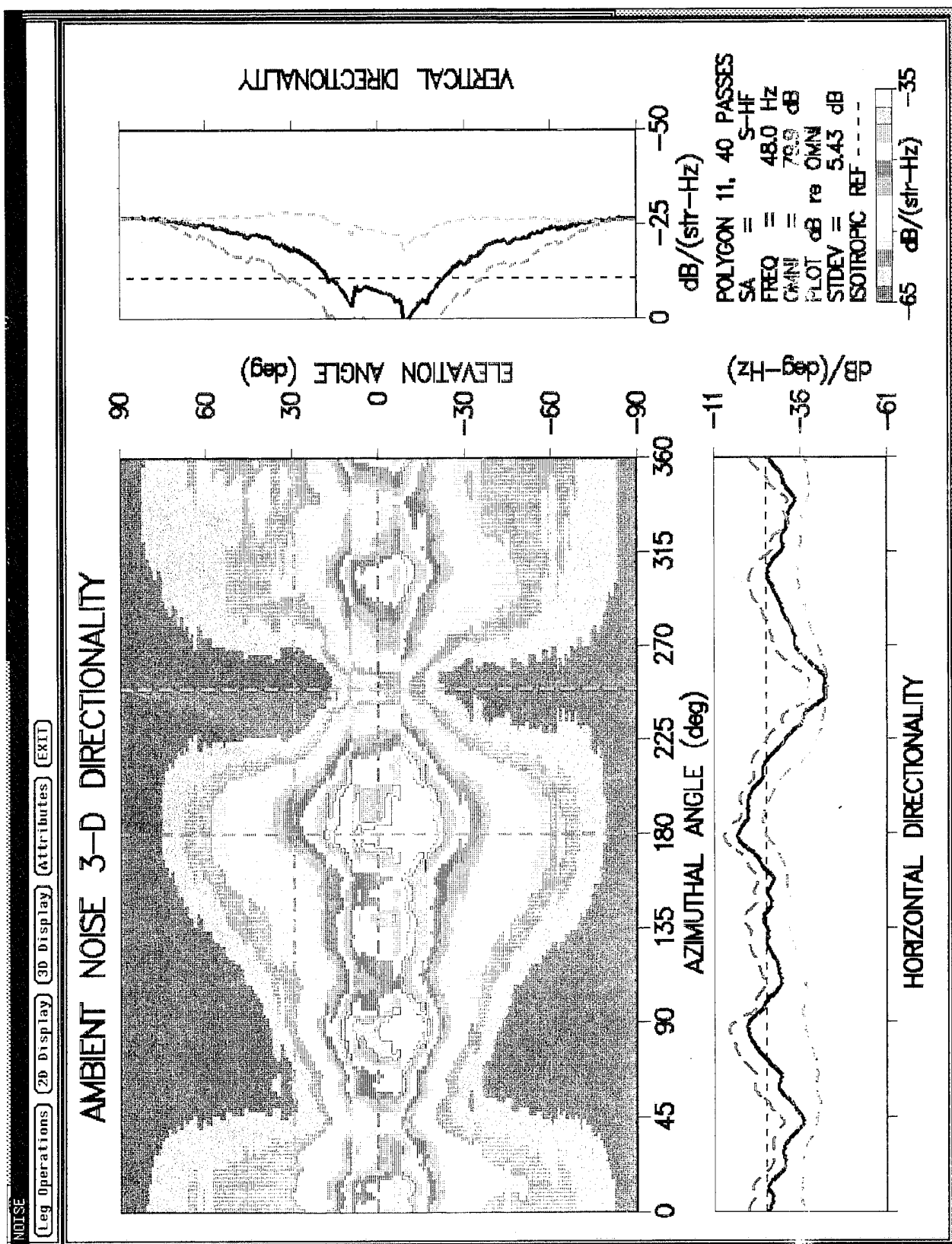
Figure A2   Ambient noise 3D directionality plot for 48 Hz at site D using data from both towed line and vertical line arrays were used.
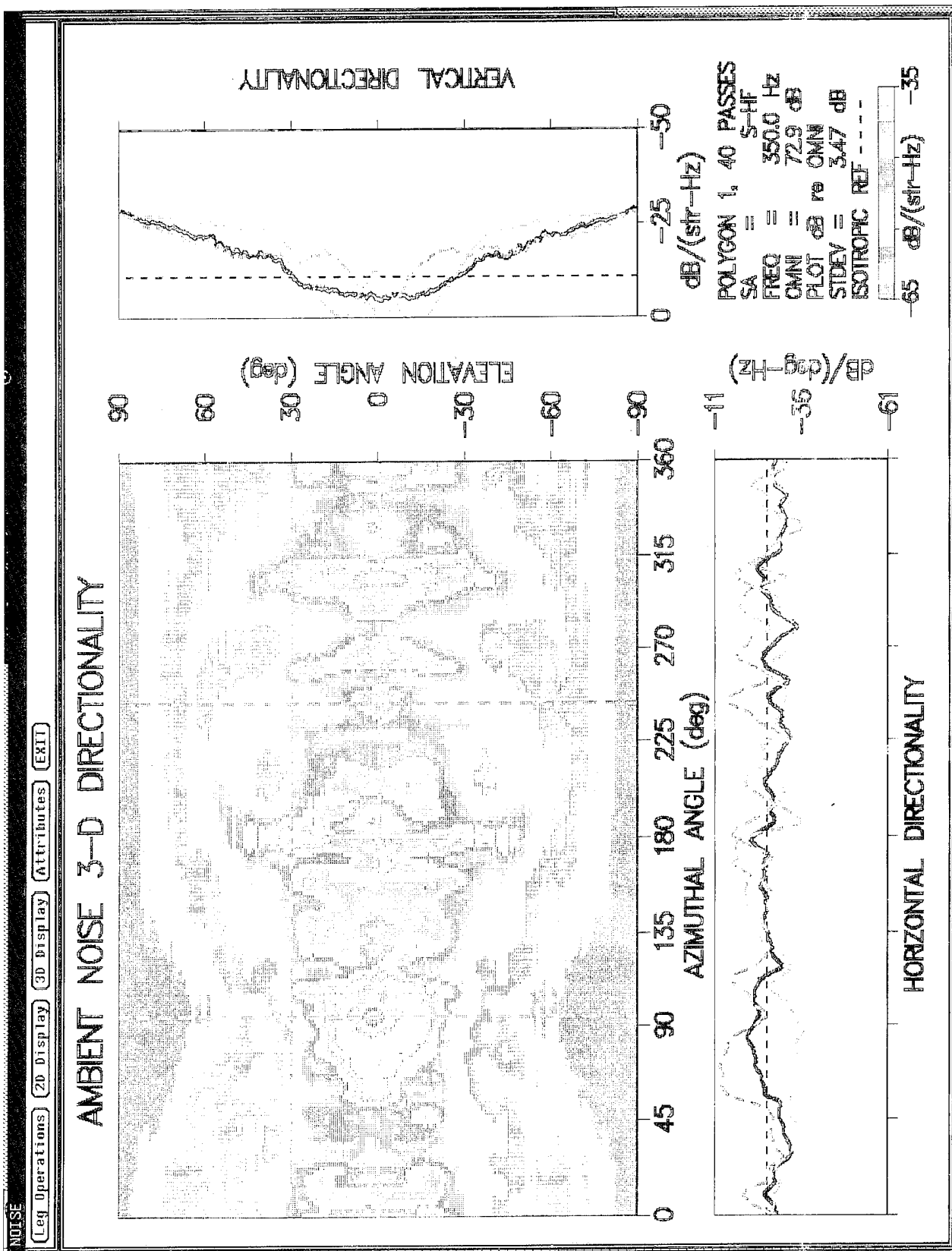
Figure A3　Ambient noise 3D directionality plot for 350 Hz at site D using data from both towed line and vertical line arrays were used.

36
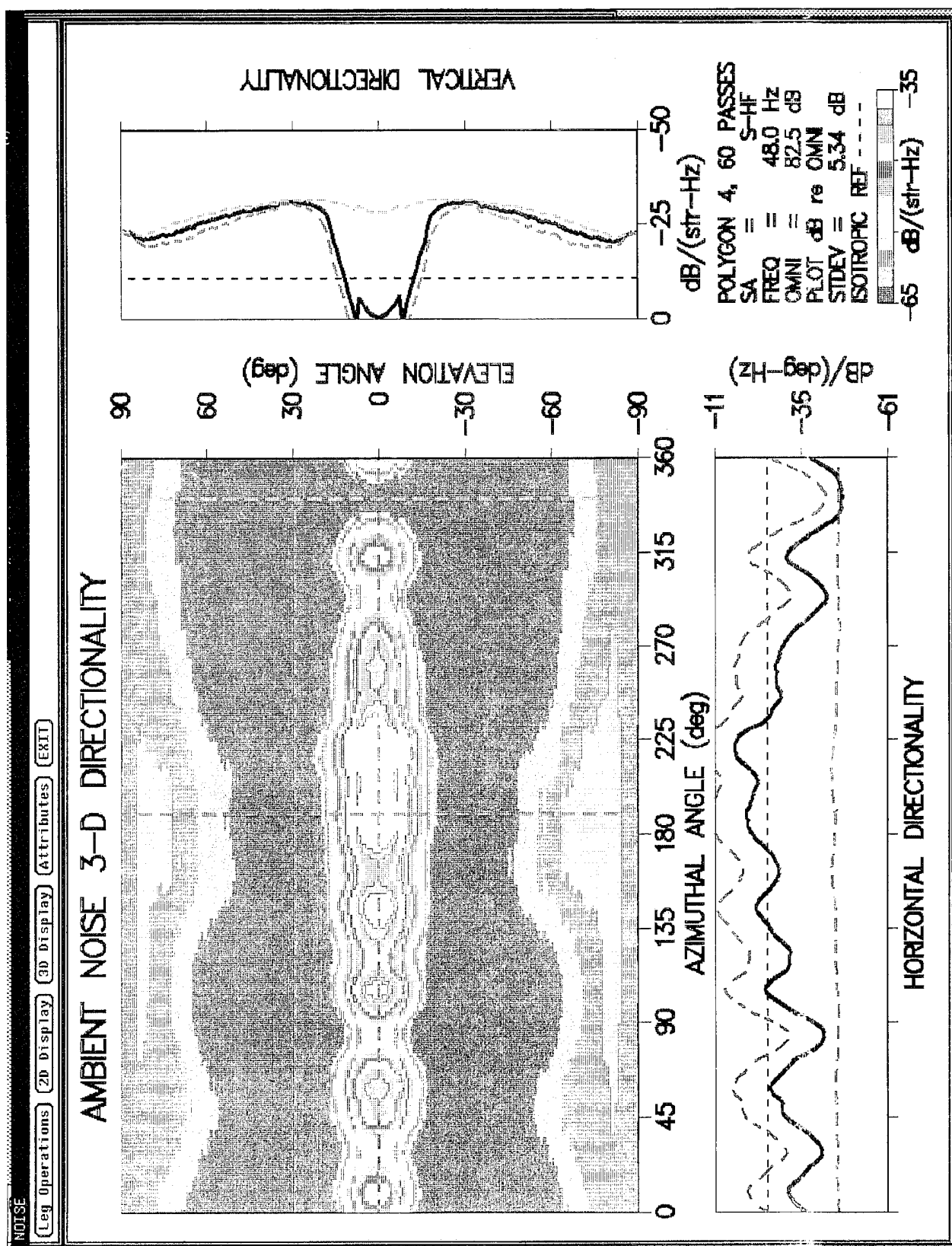
Figure A4 Ambient noise 3D directionality plot for 48 Hz at site E using data from both towed line and vertical line arrays were used.

Figure A5 Ambient noise 3D directionality plot for 350 Hz at site E using data from both towed line and vertical line arrays were used.
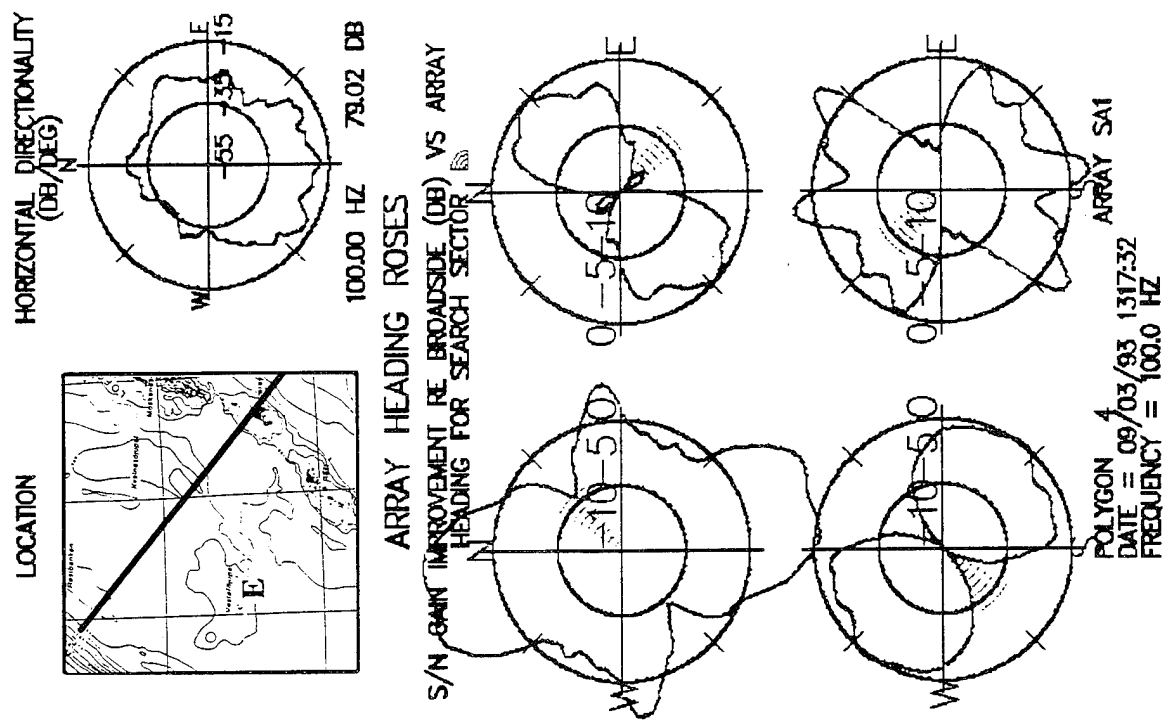
Figure A6 Array Heading Rose plots, corresponding noise rose, and geographic location for site E for 100 Hz.
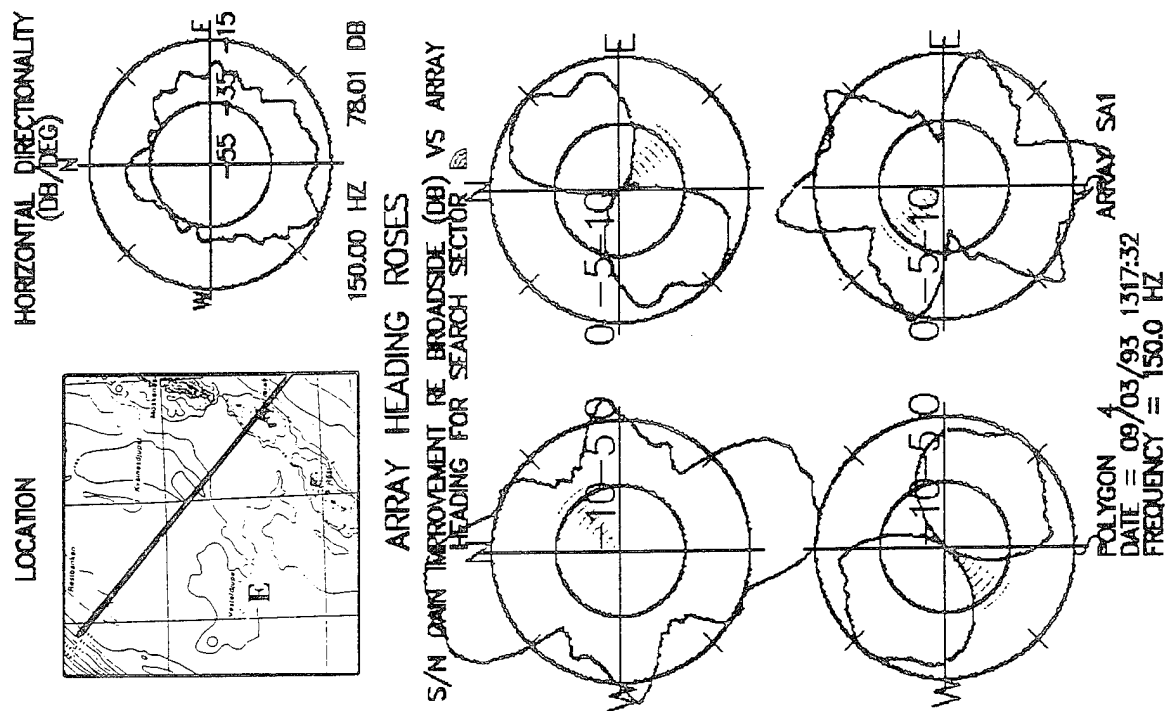
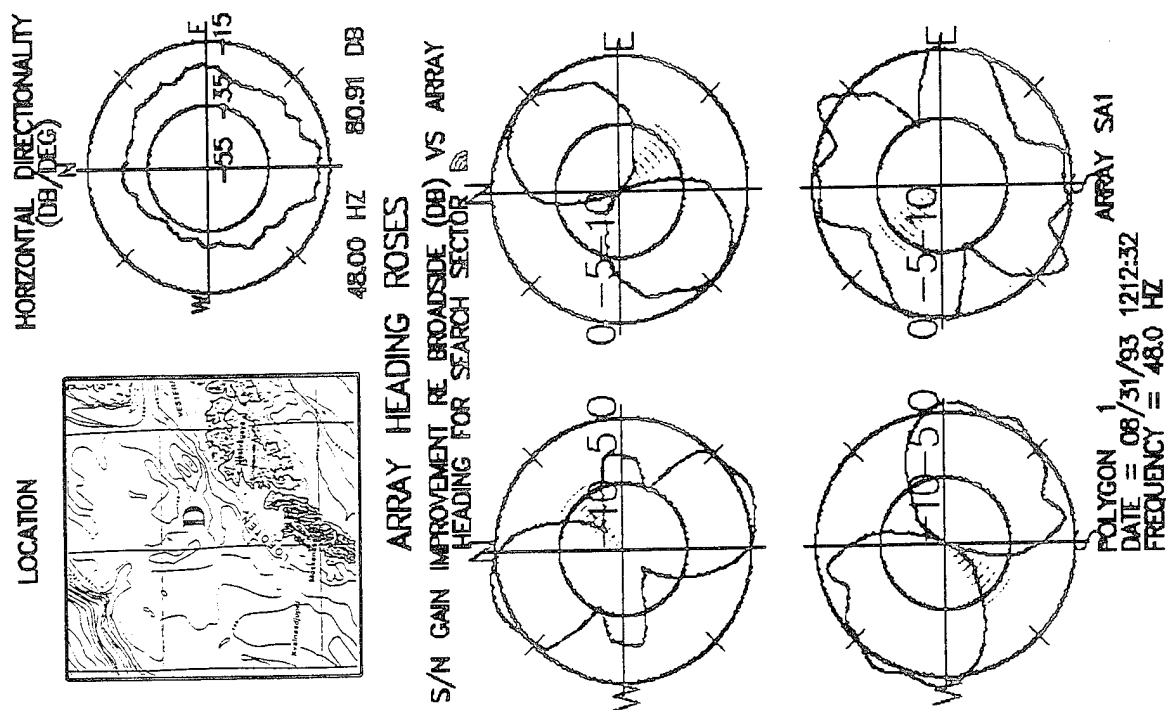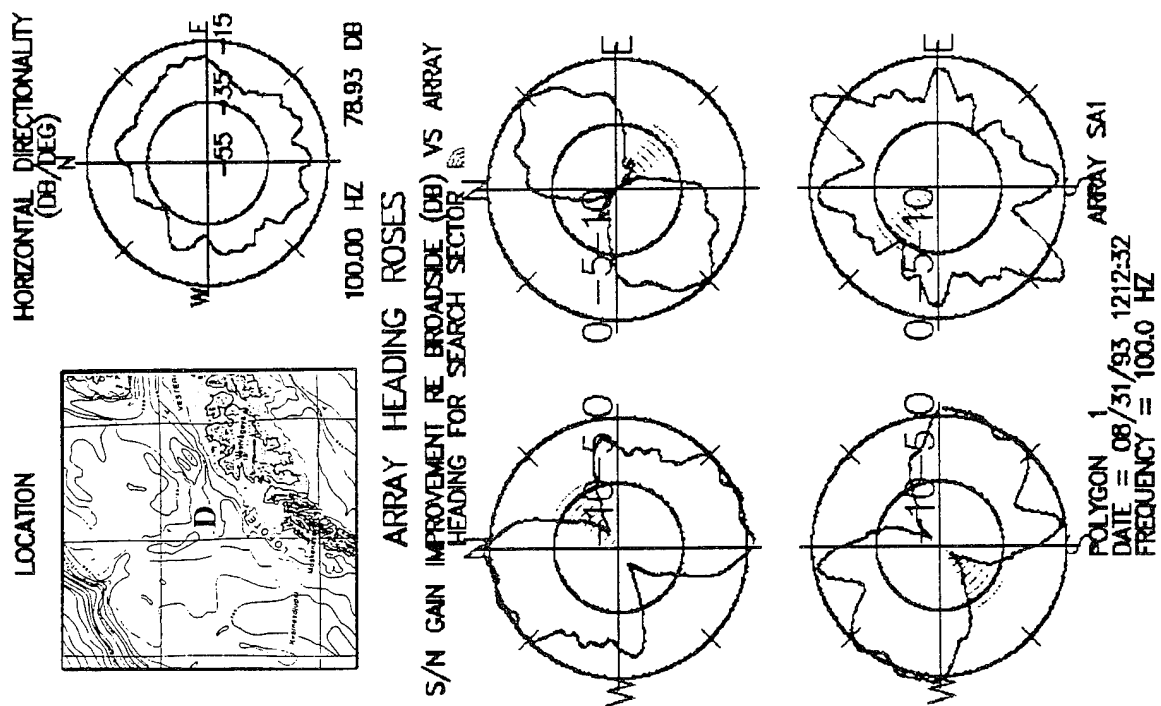Figure A7   Array Heading Rose plots, corresponding noise rose, and geographic location for site E for 150 Hz.
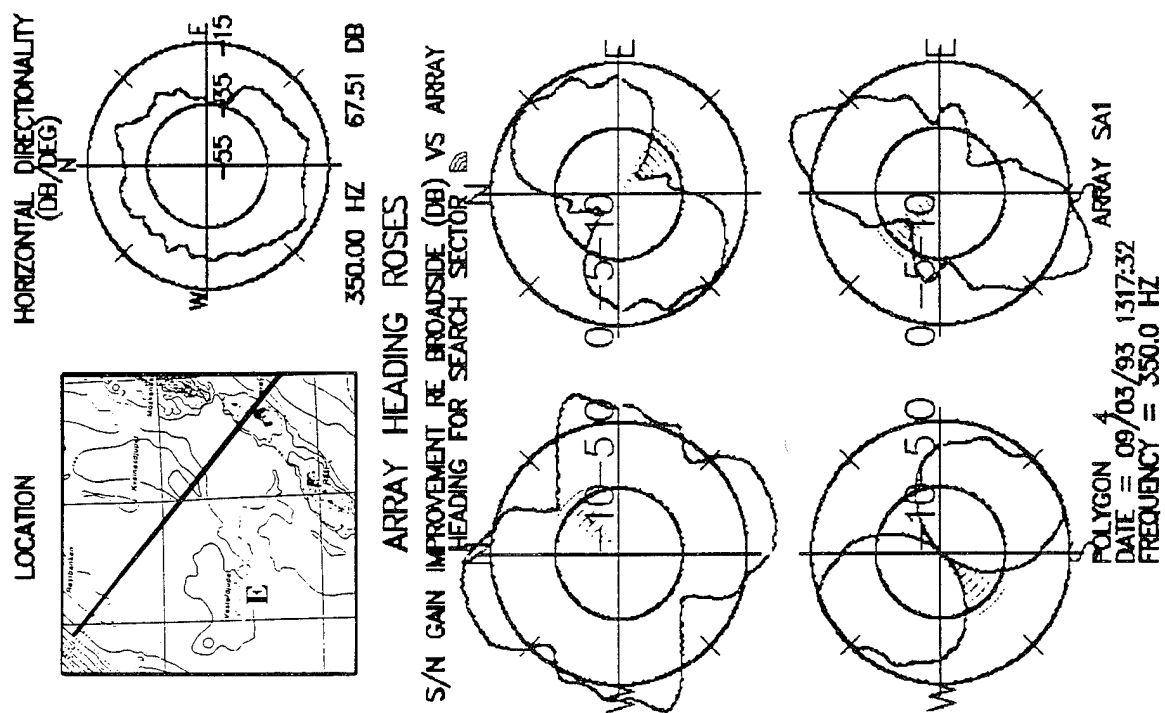
Figure A8   Array Heading Rose plots, corresponding noise rose, and geographic location for site E for 350 Hz.

41

Figure A9 Array Heading Rose plots, corresponding noise rose, and geographic location for site A for 48 Hz.

Figure A10 Array Heading Rose plots, corresponding noise rose, and geographic location for site A for 100 Hz.
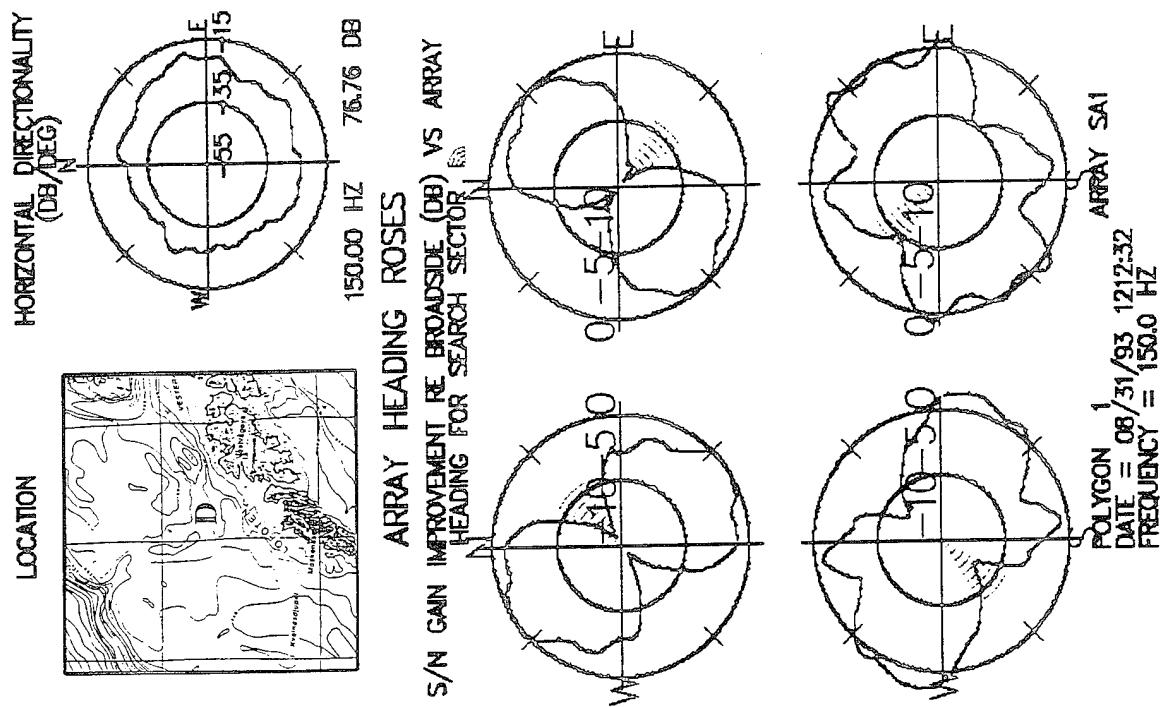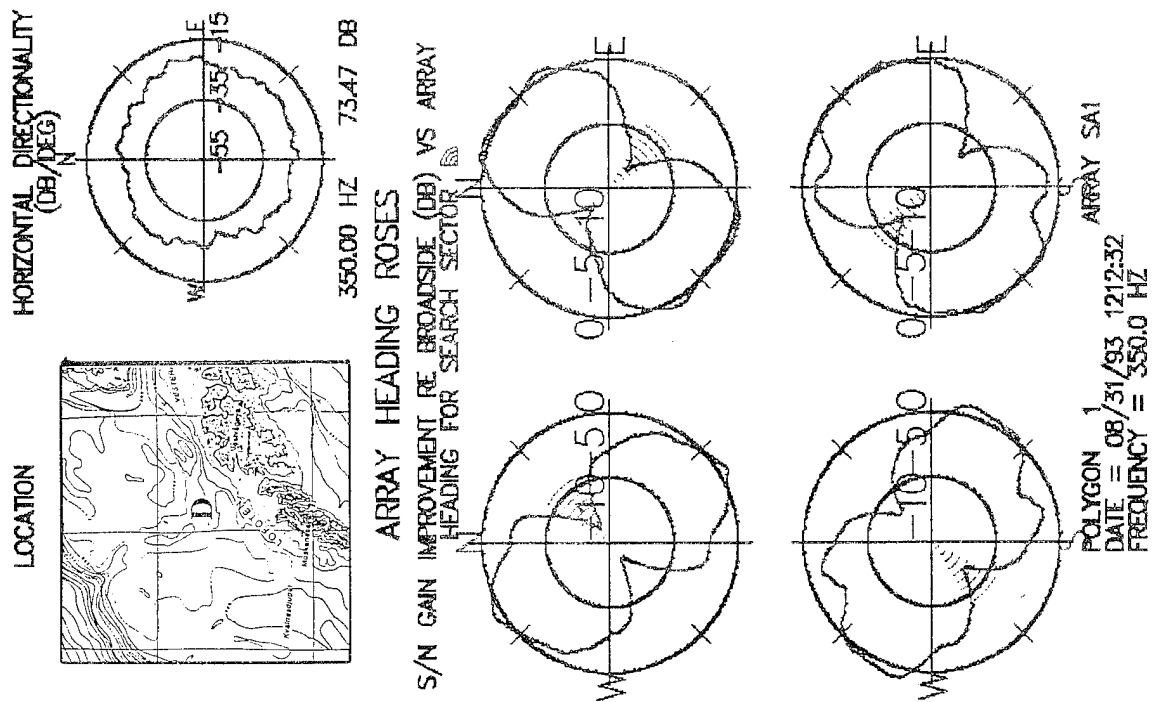
LOCATION

HORIZONTAL DIRECTIONALITY
(DB/DEG)

150.00 HZ   82.18 DB

ARRAY HEADING ROSES

S/N GAIN IMPROVEMENT RE BROADSIDE (DB) VS ARRAY
HEADING FOR SEARCH SECTOR

ARRAY SA1

POLYGON 7
DATE = 09/08/93 0733:02
FREQUENCY = 150.0 HZ

Figure A11   Array Heading Rose plots, corresponding noise rose, and geographic location
for site A for 150 Hz.

44
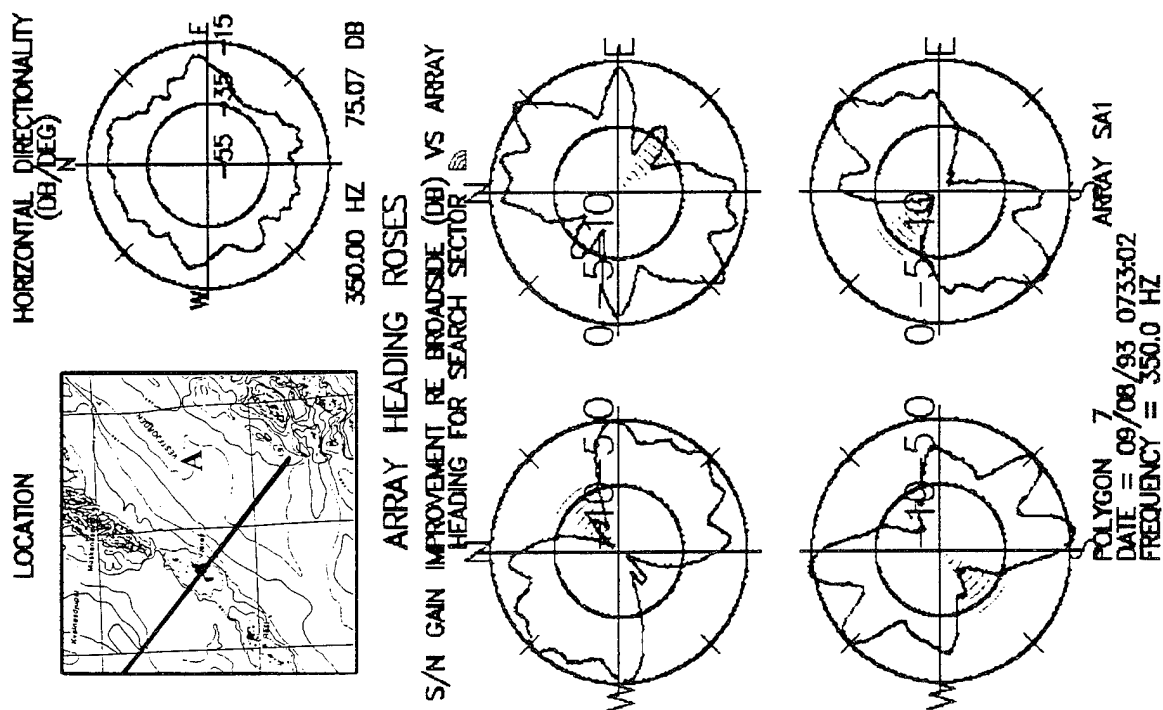
Figure A12   Array Heading Rose plots, corresponding noise rose, and geographic location for site A for 350 Hz.

45

Figure A13   Array Heading Rose plots, corresponding noise rose, and geographic location
for site D for 48 Hz.

Figure A14 Array Heading Rose plots, corresponding noise rose, and geographic location for site D for 100 Hz.

Figure A15 Array Heading Rose plots, corresponding noise rose, and geographic location for site D for 150 Hz.

Figure A16 Array Heading Rose plots, corresponding noise rose, and geographic location for site D for 350 Hz.
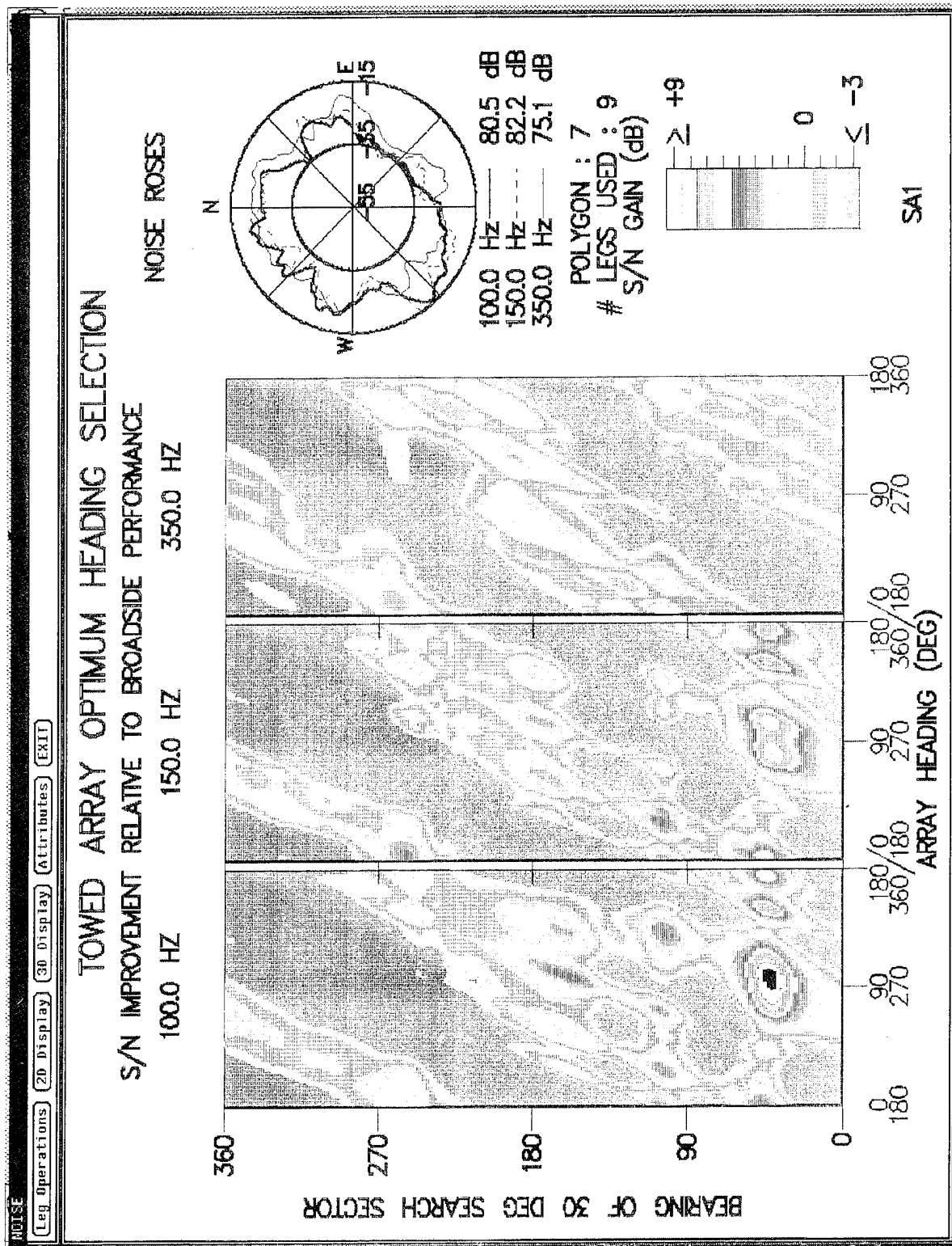
Figure A17 Array Heading Surfaces for 100 Hz (left), 150 Hz (middle), and 350 Hz (right), at site A with corresponding noise roses (top right hand corner). The omnidirectional levels are included opposite the frequency beneath the noise roses.
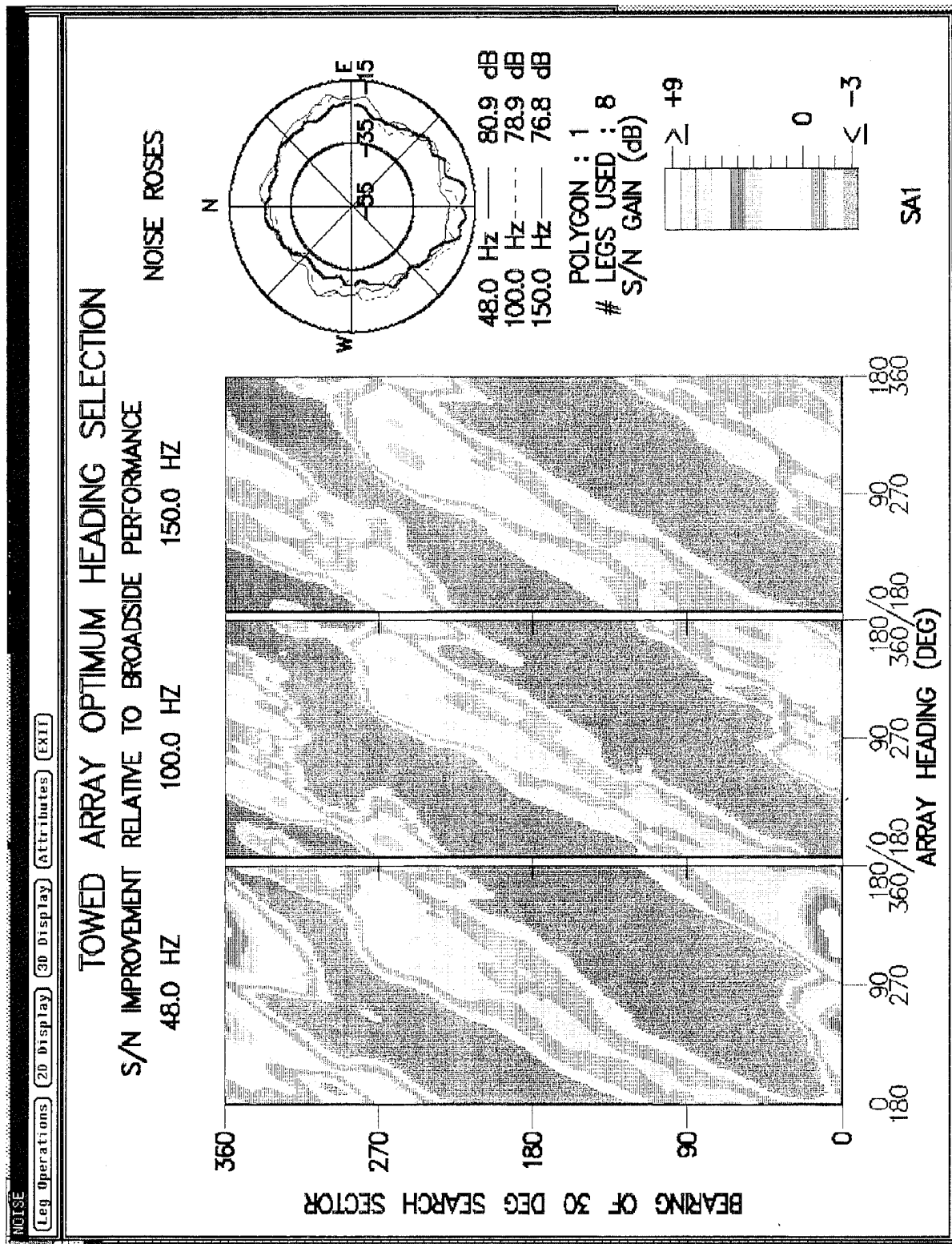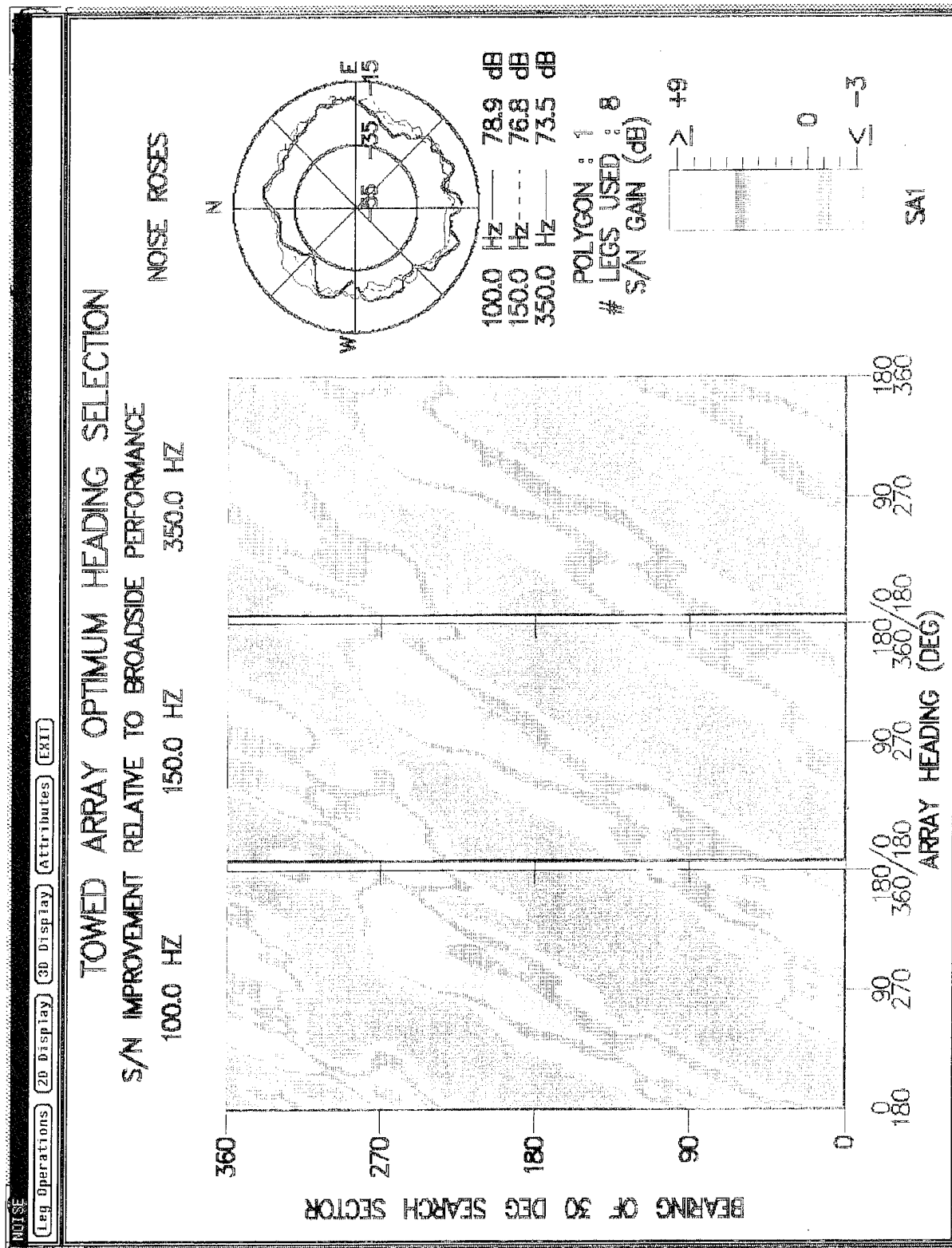
50

Figure A18 Array Heading Surfaces for 48 Hz (left), 100 Hz (middle), and 150 Hz (right), at site D with corresponding noise roses (top right hand corner). The omnidirectional levels are included opposite the frequency beneath the noise roses.

Figure A19 Array Heading Surfaces for 100 Hz (left), 150 Hz (middle), and 350 Hz (right), at site D with corresponding noise roses (top right hand corner). The omnidirectional levels are included opposite the frequency beneath the noise roses.
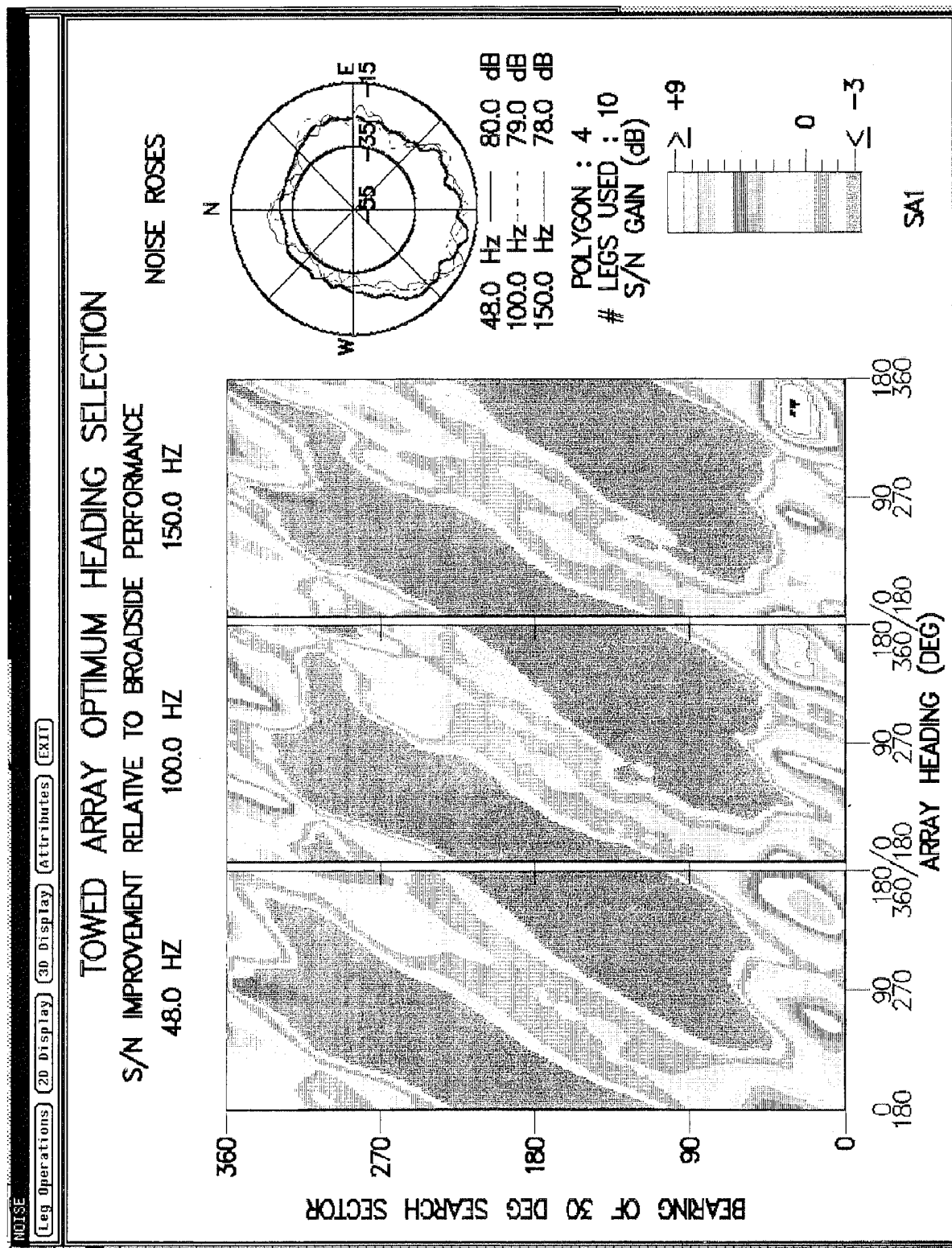
Figure A20 Array Heading Surfaces for 48 Hz (left), 100 Hz (middle), and 150 Hz (right), at site E with corresponding noise roses (top right hand corner). The omnidirectional levels are included opposite the frequency beneath the noise roses.
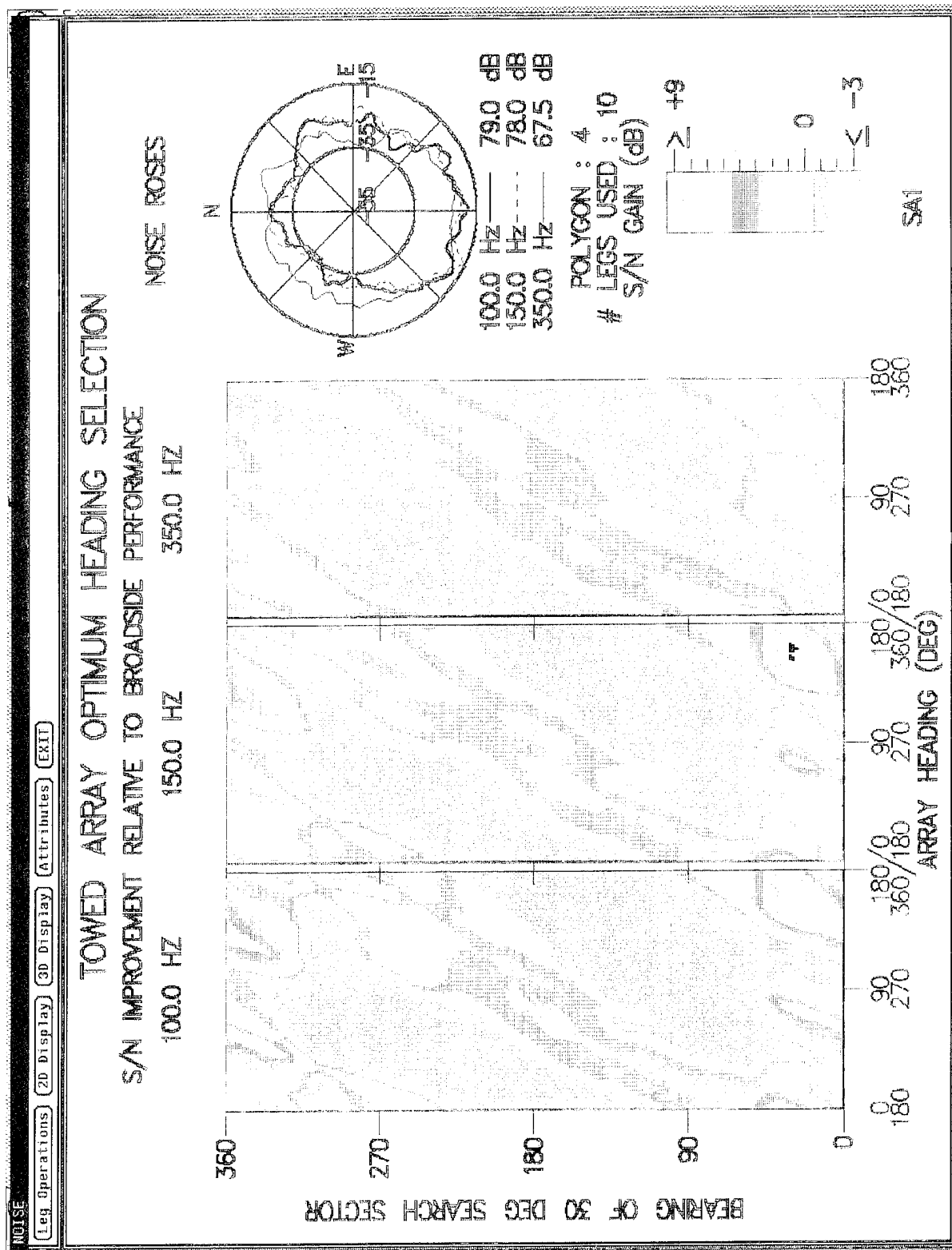
Figure A21 Array Heading Surfaces for 100 Hz (left), 150 Hz (middle), and 350 Hz (right), at site E with corresponding noise roses (top right hand corner). The omnidirectional levels are included opposite the frequency beneath the noise roses.